AD-A083 721 TEXAS A AND M UNIV COLLEGE STATION MECHANICS AND MAT--ETC F/G 11/4
COMPOSITE MATERIALS FOR STRUCTURAL DESIGN.(U)
FEB 80 R A SCHPEY F49620-78-C-0034
UNCLASSIFIED MM-3724-80-1 AFOSR-TR-80-0307 NL

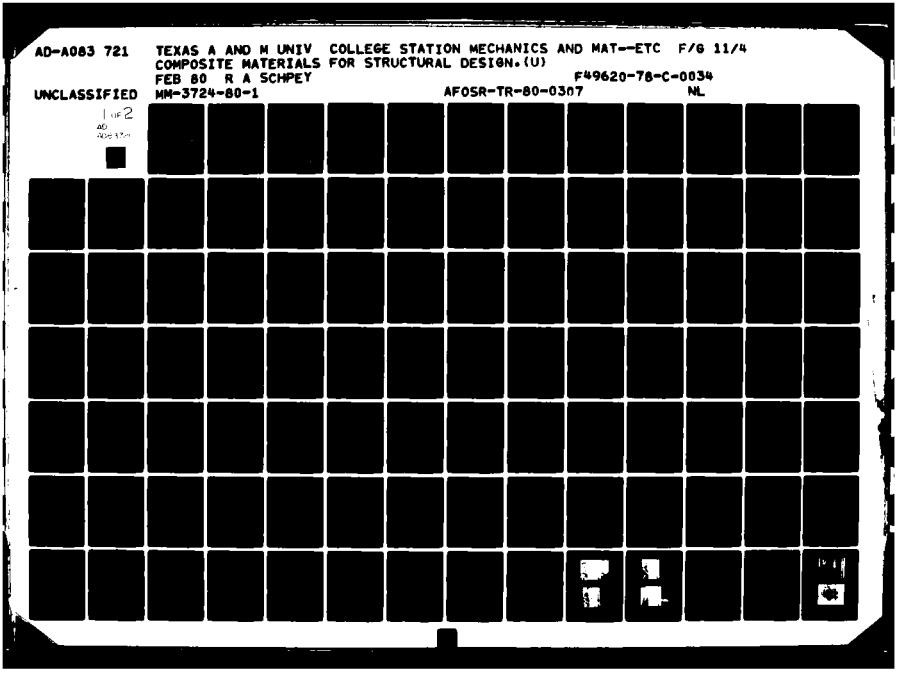

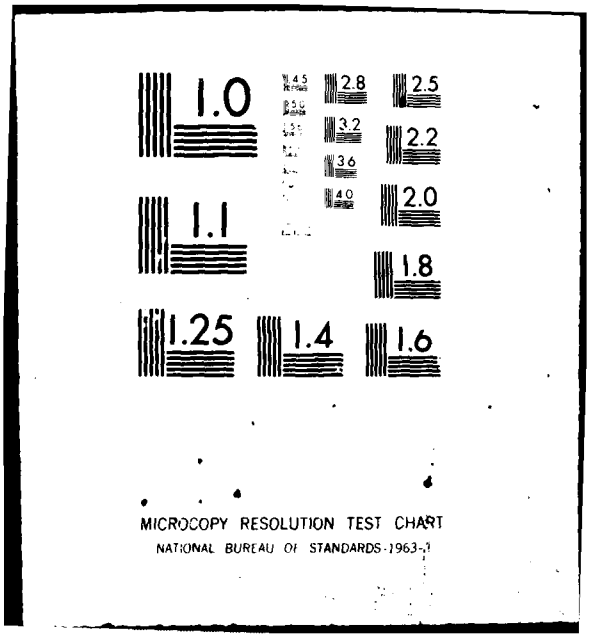
1.0
1.1
1.25
1.4
1.6
1.8
2.0
2.2
2.5
2.8
3.2
3.6
4.0
MICROCOPY RESOLUTION TEST CHART
NATIONAL BUREAU OF STANDARDS-1963-A

Mechanics and Materials Center
TEXAS A&M UNIVERSITY
College Station, Texas

COMPOSITE MATERIALS FOR STRUCTURAL DESIGN

(SECOND ANNUAL TECHNICAL REPORT)

AIR FORCE OFFICE OF SCIENTIFIC RESEARCH
OFFICE OF AEROSPACE RESEARCH
UNITED STATES AIR FORCE
CONTRACT NO. F49620-78-C-0034
FEBRUARY 1980

MM 3724-80-1

UNCLASSIFIED
SECURITY CLASSIFICATION OF THIS PAGE (When Data Entered)

REPORT DOCUMENTATION PAGE

READ INSTRUCTIONS BEFORE COMPLETING FORM

1. REPORT NUMBER: AFOSR-TR- 80-0307	2. GOVT ACCESSION NO. AD-A083 721
3. RECIPIENT'S CATALOG NUMBER	
4. TITLE (and Subtitle): COMPOSITE MATERIALS FOR STRUCTURAL DESIGN	5. TYPE OF REPORT & PERIOD COVERED: INTERIM, 15 Jan 79 - 31 Dec 79
	6. PERFORMING ORG. REPORT NUMBER: MM 3724-80-1
7. AUTHOR(s): R. A. SCHAPERY, et al.	8. CONTRACT OR GRANT NUMBER(s): F49620-78-C-0034
9. PERFORMING ORGANIZATION NAME AND ADDRESS: TEXAS A&M UNIVERSITY, MECHANICS & MATERIALS RESEARCH CENTER, COLLEGE STATION, TX 77843	10. PROGRAM ELEMENT, PROJECT, TASK AREA & WORK UNIT NUMBERS: 2307/B1, 61102F
11. CONTROLLING OFFICE NAME AND ADDRESS: AIR FORCE OFFICE OF SCIENTIFIC RESEARCH/NA, BLDG 410, BOLLING AIR FORCE BASE, D C 20332	12. REPORT DATE: February 1980
	13. NUMBER OF PAGES: 29 + Appendices
14. MONITORING AGENCY NAME & ADDRESS (if different from Controlling Office)	15. SECURITY CLASS. (of this report): UNCLASSIFIED
	15a. DECLASSIFICATION/DOWNGRADING SCHEDULE

16. DISTRIBUTION STATEMENT (of this Report)

Approved for public release; distribution unlimited.

17. DISTRIBUTION STATEMENT (of the abstract entered in Block 20, if different from Report)

18. SUPPLEMENTARY NOTES

19. KEY WORDS (Continue on reverse side if necessary and identify by block number)

COMPOSITE MATERIALS	THERMOMECHANICAL BEHAVIOR OF RESINS	
PROCESSING OF LAMINATES	THERMOMECHANICAL BEHAVIOR OF COMPOSITES	
RESINS	DELAMINATION	
ADHESIVES	FINITE ELEMENTS	NEUTRON RADIOGRAPHY
VISCOELASTICITY	AGING OF RESINS	AEROELASTIC TAILORING

20. ABSTRACT (Continue on reverse side if necessary and identify by block number)

Summarized are research activities related to polymer-matrix composite materials in the areas of processing and dynamic mechanical testing, physical aging, delamination fracture characterization, temperature and moisture effects, finite element modelling of nonlinear viscoelastic materials, and neutron radiography. Also included are Abstracts of five M.S. theses and six papers describing several recently completed experimental and analytical research investigations of factors which pertain to processing, testing, and design of composite structures.

DD FORM 1 JAN 73 1473

UNCLASSIFIED

COMPOSITE MATERIALS FOR STRUCTURAL DESIGN.

Second Annual Technical Report, no 2, 15 Jan – 31 Dec 79,

by the

Professional Staff

of the

TEXAS A&M UNIVERSITY

Mechanics and Materials Research Center

Submitted to the

Air Force Office of Scientific Research

Office of Aerospace Research

United States Air Force

MM-3724-80-1

Contract No. F49620-78-C-0034

Feb[redacted]80

TABLE OF CONTENTS

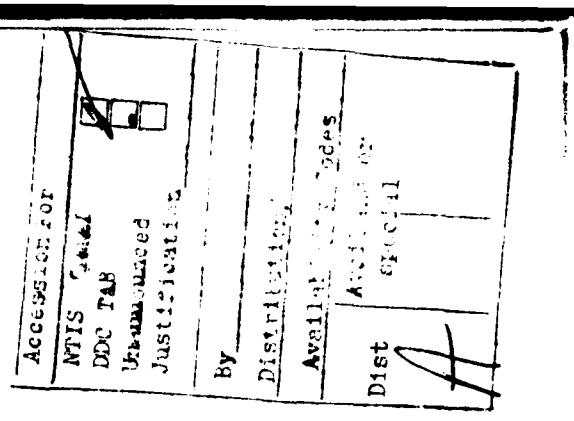

1. INTRODUCTION

1.1 Summary

Primary activities during the second year consisted of (i) expanding the laboratory capabilities for processing and testing of composites, (ii) conducting research in accordance with the Statement of Work given in Section 1.3, (iii) preparing nine technical papers and M.S. theses, and (iv) various interactions of the faculty with the technical community through presentation of papers, participation as members of technical committees, etc.

Sections 2 - 5 summarize the research activities. The professional personnel associated with the project and the outside activities of the faculty related to composites are given in Section 6. Papers completed and/or published during the year are reproduced in Appendix A. A brochure describing the student activities is in Appendix B.

1.2 Discussion

The general objective of the research program is to develop improved understanding of structural composite material as a basis for improving its structural performance. Integral to achievement of this objective is the determination of constitutive equations and time (or cycles) to fracture for complex loading patterns and hostile environments such as high relative humidity. This in turn will require a better understanding of the viscoelastic deformation and micromechanisms of fracture in composites including delamination, cumulative damage via microcrack initiation and growth, and meaningful failure criteria. The importance

of micromechanisms of viscoelastic deformation and fracture in epoxy materials has only recently become widely appreciated; for example, graphite/epoxy composites are quite sensitive to processing and to service environments, especially moisture [1]. Furthermore, because curing is seldom taken to completion in the epoxies used in graphite/epoxy composites [2], the degree of cure is a processing variable. Physical aging of the epoxy matrix may occur in service, giving significant changes in mechanical properties [3]. The post-cure cool-down path affects the magnitude of residual stresses in a composite [4]. Moisture absorption can change the glass transition temperature, giving a significant change in mechanical properties [1]. The rate of moisture absorption appears to depend on the degree of curing and physical aging (densification), and moisture content may itself affect the rate of physical aging.

The lack of consistency in experimental results and micromechanistic modelling in the epoxy matrix composite materials literature today is a consequence of the fact that much of the earlier research was conducted without fully controlling some of the more subtle variables. It is anticipated that the continuing research program at Texas A&M University described herein will make a major contribution toward a more unified understanding of composite materials behavior.

In view of the large number of variables to be considered, it is essential that the mechanical testing be guided by mechanistic modelling to keep the total amount of experimental work at a manageable level. A considerable part of the effort at Texas A&M University is being so directed.

1.3 Statement of Work

- "a. Investigate the effects of composite cure cycle parameters on the mechanical characteristics of structural specimens and components (see Section 2.):

  (1) Investigate the development of new innovative in-process monitoring devices and study improvements in the "Duomorph" sensor.

  (2) Conduct experimental measurements on both neat resin, unidirectional laminates and cross-ply laminates to establish the relationships at various elevated temperature and relative humidities between processing parameters and mechanical strain rate behavior, linear and identified nonlinear viscoelastic behavior, dimensional stability, and fracture characterization.

  (3) Investigate the influence of processing parameters on T_g at various relative humidities.

- b. Investigate the influence of elevated temperature and high relative humidity environments on composite laminates and adhesively bonded structural components (see Section 3.):

  (1) Investigate, on a theoretical level, the formulations of a coupled diffusion theory to accurately predict the environmental degradation of composite laminates and adhesive mechanical performance which considers the influence of cure cycle parameters being investigated in a above.

  (2) Predict moisture concentration profiles and internal stress/strain fields within a laminate and bonded structure as well as in the vicinity of exposed edges. These profiles will consider generic environmental conditions of absorption and desorption.

  (3) Compare theoretical predictions with available experimental data or define experiments which would yield necessary data for this comparison.

- c. Investigate suitable experimental techniques which can be used to nondestructively examine composite laminate initial defects, damage growth and environmental degradation characteristics which affect mechanical performance. Initially, emphasis will be given to neutron radiography as a suitable technique (see Section 4):

  (1) Conduct necessary experiments to characterize neutron beam parameters and associated parameters' sensitivities applicable for nondestructively examining major composite laminate mechanical characteristics which affect strength, dynamic response and durability.

  (2) Investigate the development of experimental neutron radiography techniques to measure moisture concentrations in composite laminates as well as spatial concentration profiles.

(3) Investigate the development of automated procedures for the analysis of data from neutron radiography experiments which accurately and efficiently characterize and identify laminate initial defects, mechanical damage, and moisture concentrations.

(4) Investigation of automated data analysis procedures in c(3) above will consider both planar and stereographic data displays."

2. PROCESSING AND TESTING OF RESIN AND COMPOSITES

2.1 New Equipment

The processing and testing capability is being expanded through the acquisition of a large amount of new equipment. Recently acquired is a MINC-11 laboratory data acquisition and control microcomputer system (manufactured by Digital Equipment Corporation) and a digital plotter to provide high quality, permanent graphic output. Orders have been placed for 1) curing oven, 2) vacuum oven, 3) automatic controls for use on existing press/autoclave, 4) cold stage for differential scanning calorimeter, 5) diamond tools for machining composites, 6) humidity monitor, 7) digital thermometer, and 8) laboratory oscilliscope. Funds were provided by AFOSR and Texas A&M University.

A considerable amount of additional testing and data acquisition equipment is to be purchased during the coming year including a closed-loop MTS mechanical testing system, two data acquisition and microcomputer systems, digital oscilliscope and an ultrasonic tester with C-scan capability. Funds are to be provided by Texas A&M University.

2.2 Processing of Composites

The laminating press/autoclave fabricated under the project and placed into operation last year has been used extensively. Faculty and student research assistants have learned the detailed procedure for laminating and curing a structural composite. They have used the press to fabricate specimens used in the several research tasks.

2.3 Data Analysis

The laboratory data acquisition system has been used to gather data from creep and recovery experiments. Data analysis software employing a nonlinear Gauss iteration technique for estimating parameters in the following representations for creep compliance was developed:

$$D(t) = D_0 + D_1 t^n, \quad D(t) = D_0 + D_1 \log t, \quad \text{and} \quad D(t) = D_1 t^n$$

Many plotting routines have been developed which produce high quality and high resolution graphic presentations of data. Figure 1 is an example.

2.4 Dynamic Mechanical Response of Resins and Composites

This portion of the study on the effect of cure cycle parameters is concerned with the direct monitoring of the viscoelastic complex modulus of resins and composites during and immediately following the cure cycle. We have adapted a piezoelectric device called the "duomorph" for such use.

The duomorph consists of two crystalline piezoelectric plates which are bonded together; a central metallic plate is sometimes used to alter the response characteristics of the assembly. The duomorph is electrically excited and, through a study of its bending response when in contact with a material of interest, the viscoelastic properties of this material are obtained. The gage was originally developed for the purpose of measuring in situ complex modulus when embedded in the fuel in a solid propellant rocket [5]; for this application, which involved telemetry to trigger and measure the gage response, one piezoelectric plate was employed as a

SYMBOL	TEMP(C)	STRESS(MPA)	T PRIME(SEC)	CYCLE #	SPEC #
■	23.9	1.66200E+07	640	7	B16
●	40.6	1.66200E+07	640	7	B16
▲	57.2	1.64900E+07	640	7	B16
+	76.6	1.66200E+07	640	7	B16
×	93.3	1.66200E+07	640	7	B16

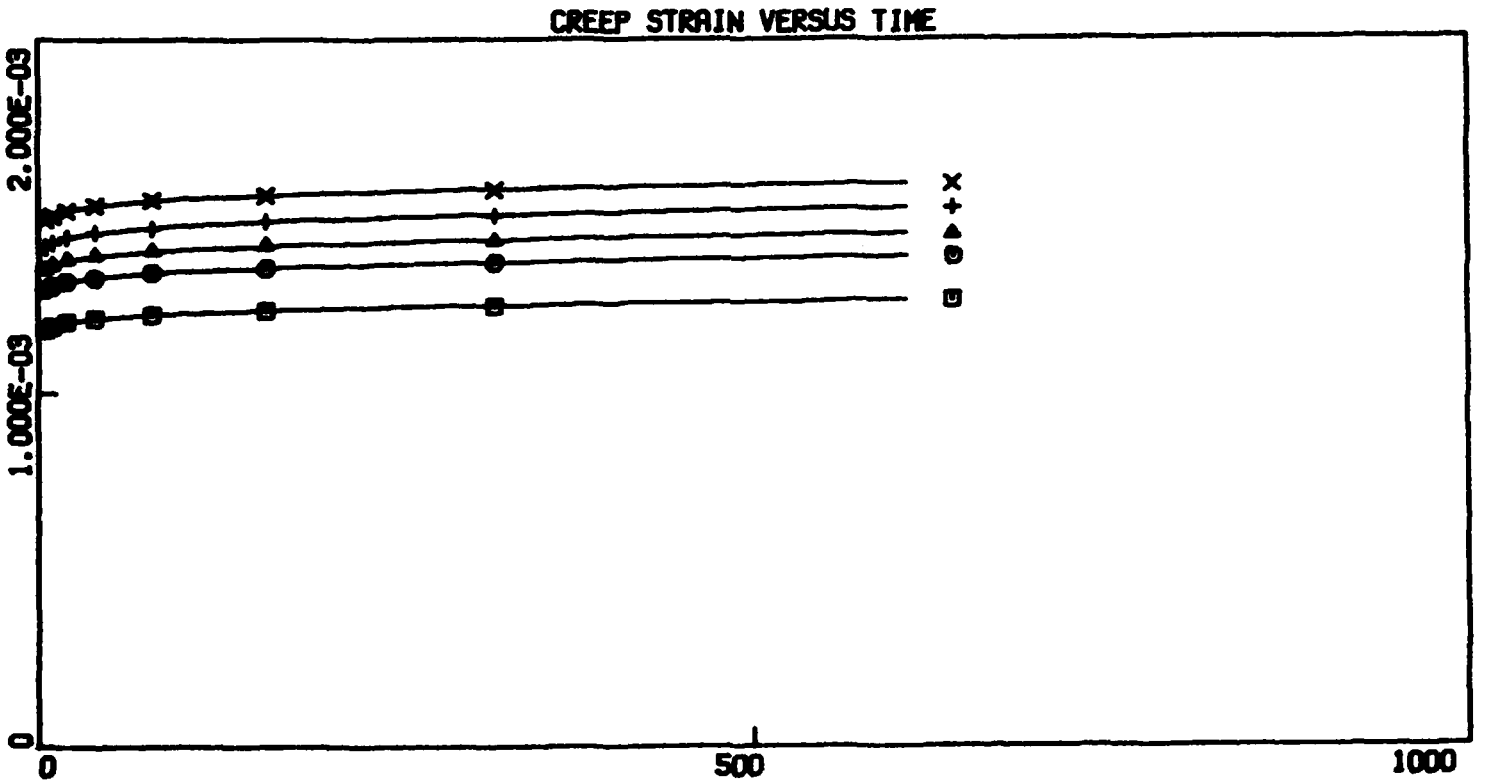

Figure 1: Creep strain as a function of time.

driver and the voltage response of the other was used to obtain the strain response.

The latest version of the duomorph developed on the project has been demonstrated to perform reproducibly in air over the temperature range of 25 to 180°C, the upper limit being the approximate cure temperature for advanced composites.

It consists of two 1 inch diameter x 0.010 thick piezoelectric discs bonded together using a conductive epoxy. Evaluation of piezoelectric material from different suppliers has resulted in the selection of a new material, K-350, which is a lead zirconate titanate piezoelectric ceramic manufactured by Keramos, Inc., Lizton, Indiana. As with the gage used in the study of propellant, one plate serves as a driver and one as a response transducer. However, in order to obtain complex moduli with sufficient accuracy for use with stress analysis, we have found it necessary to work with the input and response current, rather than voltage, in deriving complex moduli.

Tests of Hercules 3501-6 epoxy and a room-temperature cure epoxy resin were sufficiently successful to justify further refinements by upgrading the input/response electronics and the addition of an automated data acquisition system (which will include a Fast fourier transform analysis capability). Necessary equipment will be ordered during the next quarter. Also, it is planned to adapt the gage for use with laminates and develop the necessary additional theoretical analysis and experimental techniques. The high stiffness of composites compared to the neat epoxy will probably require some new piezoelectric (PZT) elements and gage design. One possibility would be a PZT gage

mounted in a recessed cavity in the bottom metal plate which supports the laminate during cure. The gage would rest on a relatively soft layer so that the only resistance to stretching and bending would arise from contact with the laminate. The PZT material would be polarized so as to deform primarily in one direction, and the gage would be placed so that it is at 90° to the fiber direction of the bottom ply. Through analysis and calibration, the amount of bending and stretching will be used to extract the insitu complex modulus of the epoxy, or at least a relative measure of this modulus. It is expected that before and during gelation, the changes in bending resistance will be most sensitive to resin changes. However, little bending will occur after the resin is very stiff, and then the amount of stretching will be the best indicator of resin change. Initially, unidirectional layups will be employed. After the method is developed for this special case, laminates with various ply orientations will be monitored; with the intent of using the gage response in a closed-loop control of the press/autoclave.

2.5 Physical Aging of Epoxy Resins

The study of aging phenomena following curing and quenching from the glass-transition temperature T_g is continuing. The resin matrix of the composite is below the glass transition in use and so continues to change properties with time due to a relaxation of the free volume toward its equilibrium value. These changes can be observed in a variety of ways; we are doing it primarily by measuring the specific heat curve near T_g in the differential scanning calorimeter (DSC) and by studying the creep and recovery behavior of flexure samples in the thermo-mechanical

analyzer (TMA). Some preliminary investigations with the duomorph (cf. Section 2.4) indicate that this device will prove useful in the study of aging, and therefore this approach will be further explored during the coming year.

The changes in the specific heat which we observe are quantities which can be related to several molecular models of the glass transition, which imply that the mechanical characteristics such as brittleness will also change in time. Such changes would be of importance in composite materials since aging has been found to continue over many decades of time in other thermosetting materials. Any mechanical characteristics of the composite which depend upon the brittleness of the resin can be expected to evolve over a matter of years if our suppositions are correct. A variety of resins have been studied, which includes the proprietary resins as well as a number where the crosslink density can be estimated. The work is tedious since moisture content, completeness of cure, and other factors also influence the same experimental quantities. However, the work is sufficiently far along that we expect to be able to prepare a technical report on the DSC studies during the next quarter.

The aging studies conducted with the TMA are described in the M.S. Thesis "Determination of the Relationship of Free Volume to Mechanical Behavior for an Epoxy System Subjected to Various Aging Histories" (cf. Section 5.2).

2.6 Mechanical and Failure Properties of Composites Including Environmental Effects

Various investigations have been completed and are reported in M.S. Theses (cf. Section 5.2) and in the paper "A Method for Determining the

Mode I Delamination Fracture Toughness of Elastic and Viscoelastic Composite Materials", which appears in Appendix A.

Further work on mechanical and failure properties will be conducted during the coming year, as indicated in the list of M.S. Thesis topics in Section 5.1.

3. ANALYSIS OF COMPOSITES

3.1 Summary

Many analytical results have been obtained for elastic and viscoelastic stresses and deformations due to moisture and temperature changes in composite materials and for optimum cooling paths following cure; they are covered in papers given in Appendix A and the M.S. Thesis "Stresses due to Environmental Conditioning of Cross-Ply Graphite/Epoxy Laminates" (cf. Section 5.2). Energy release rate analysis of nonlinear cantilever beams was conducted in support of the delamination fracture toughness studies (cf. Section 2.6).

During the coming year elastic and viscoelastic stress analyses and fracture analysis of composites will be conducted in combined theoretical-experimental investigations. The experimental work will serve to confirm theoretical predictions and guide the development of theoretical models for nonlinear viscoelastic mechanical behavior, physical aging, environmental effects, and damage growth and fracture. Student M.S. Thesis topics listed in Section 5.1 indicate the primary investigations to be undertaken.

In addition to analytical work, a finite element model for the prediction of nonlinear viscoelastic response of polymeric composites and other materials is under development, as discussed below.

3.2 Nonlinear Finite Element Model

A nonlinear finite element model [6] was generalized in the previous reporting period to nonlinear viscoelastic behavior using the two-

dimensional plane stress/plane strain/axisymmetric case and programmed into the AGGIE I computer program [7]. The current version of the model allows several alternate input options. The material model may be either nonlinear viscoelastic or linear viscoelastic and includes as a special case linear thermoreologically simple behavior. The input for the nonlinear material parameters $g_1(\sigma)$, $g_2(\sigma)$ and $a_\sigma(\sigma)$ (see [6] for their description) may be in terms of either tabular data or equation form as a function of stress. The computer coding has been checked thus far by running two-dimensional cases which degenerate to a uniaxial stress state.

Further work will include verification of the model for two-dimensional stress states and extension of the model so that material properties are functions of other parameters, e.g., temperature and moisture. The AGGIE program allows for general continuum analysis through the use of 4 to 8 isoparametric elements. Hence, the program will allow the solution of many geometries, including laminated composites. Future work will consider such applications. It is also intended that the nonlinear viscoelastic properties obtained in experimental investigations during the coming year will be used with this finite element code to predict response of composites to mechanical and environmental inputs.

4. NEUTRON RADIOGRAPHY

4.1 Summary

Last year the Nuclear Science Center developed an extremely high quality neutron radiography facility at the research nuclear reactor at Texas A&M University. The operational parameters such as geometric resolution, beam uniformity, film density, and neutron flux were optimized to a point where variation in material density of less than 0.5% may be measured. A variety of laminate sections with known moisture content were radiographed in an attempt to establish a relationship between film density changes for increased moisture in the samples. A laminate with known defects was also studied.

This year studies were directed toward the improvement and standardization of the sensitivity of neutron radiography to absorbed water in laminates. By using polyethylene to simulate water, it was estimated that at least 1% absorbed water was required for detection. Subsequent studies with laminates saturated to this level indicated that an even greater amount of moisture was needed. Inasmuch as the moisture level requirements for detection of moisture gradients are well above what can be expected in laminates in realistic environments, it was decided to terminate this area of investigation. However, because metals are transparent to the neutron beam while materials with hydrogen are not, this facility should be very useful for flaw detection in resin and fiber reinforced resins, especially when other detection methods are made ineffective as a result of metal barriers.

4.2 Beam and Material Characteristics

The final values of beam parameters that have been reached as a result of the research effort are:

Thermal neutron flux	$>10^7$ n/cm^2/sec
Scattered and fast neutron content	10%
Gamma intensity	$4.0 \times 10^6 \frac{n/cm^2}{mr}$
Beam uniformity	$\pm 3.5\%$
Beam divergence	1.5°

Also, optimum film developing, handling and inspection procedures necessary for reproducible data collections have been established.

Effective neutron cross sections for all of the materials studied were measured and are listed below:

Material	$\Sigma t(cm^{-1})$
Scotch ply (GL/E)	1.178
Neat Resin (1)	1.106
(2)	0.648
Defect Test Plate (GR/E)	0.179
Polyethylene	1.084
Water	0.745

(It should be noted that these cross sections are valid for the present geometry only, i.e., relatively thin plate samples in contact with the film cassette.) Also, the relationship between film density and integrated neutron flux has been established:

$$D = e\ (-0.6035\ \Phi_R^2 + 0.1561\ \Phi_R - 0.0758)$$

where D = film density

Φ_R = Relative fluence

Note that for a sample of thickness t exposed to a neutron fluence Φ_R^0, the transmitted fluence Φ_R^t may be determined from

$$\Phi_R^t = \Phi_R^0\ e^{-\Sigma t}$$

Thus, the neutron cross sections and these two equations may be used to determine changes in sample thickness (Δt) from changes in film densities.

5. GRADUATE RESEARCH ASSISTANT ACTIVITIES

5.1 Summary

The first group of graduate engineering students to participate in the current research project entered the program in September, 1978 and completed the requirements for a degree of Master of Science in August 1979. Results of their research are reported in the following theses:

1. Devitt, F. D., "Delamination Fracture Toughness of a Unidirectional Composite."
2. Douglass, D. A., "Stresses due to Environmental Conditioning of Crossply Graphite/Epoxy Laminates."
3. Grieger, K. A., "Experimental Investigation of Moisture and Temperature Conditioning of C600/5208 Graphite/Epoxy Composite Material."
4. Ring, D. S., "Determination of the Relationship of Free Volume to Mechanical Behavior for an Epoxy System Subjected to Various Aging Histories."
5. Rogers, J. B., "Aeroelastic Tailoring of Composite Materials."

Abstracts are given in Section 5.2. Copies of the theses will be provided upon written request to the Principal Investigator (R. A. Schapery).

The second group consists of eight (8) students that started work on an M.S. degree in engineering in September 1979. The thesis topics are listed below; most studies involve both experimental and theoretical work.

1. Investigation of residual deformations and curvatures in unbalanced laminates due to cool-down from cure. Viscoelastic effects are included.

2. Investigation of residual deformations and curvatures in unbalanced laminates due to moisture sorption. Viscoelastic effects are included.
3. Nonlinear viscoelastic characterization of a graphite/epoxy composite.
4. Characterization of delamination fracture toughness and its relation to microstructure.
5. Delamination fracture due to compressive loading.
6. Development of microcracks in cross-ply laminates due to mechanical loading.
7. Prediction of microcracking and delamination in composites by the finite element method, including a study of crack stability.
8. Physical aging of epoxy resin following cooling from the glass transition temperature.

The next quarterly report will contain thesis proposals describing the research planned under each of these topics. Besides conducting this research, the students are involved in academic courses, as described in the brochure in Appendix B.

In addition to graduate students, a few select undergraduate students assist in the various research activities. The participation of these students aids in the research and helps to acquaint them with composite materials prior to enrolling in the graduate program.

5.2 Abstracts of M.S. Theses Completed in August 1979

ABSTRACT

Delamination Fracture Toughness of a Unidirectional Composite. (August 1979)

Daniel Frank Devitt, B.S. A. & A.E., Purdue University;

Chairman of Advisory Committee: Dr. W. L. Bradley

An analytical technique for reducing experimental data is developed for a unidirectional composite in order to determine the delamination fracture toughness for the crack opening mode. A unique characteristic of this data reduction technique is that the crack opening mode is isolated from the other fracture processes. Isolation of this fracture mode allows for the direct determination of the critical energy release rate (G_c) and the critical stress intensity factor (K_{IC}).

The values for the critical energy release rate and the critical stress intensity factor were calculated using linear elastic fracture mechanics coupled with nonlinear beam theory. The critical energy release rate is found from utilizing linear elastic fracture mechanics as it is related to the release of the stored strain energy in the system. Nonlinear beam theory is required to calculate the strain energy in the system, since large deflections and rotations are produced experimentally and are not accounted for in linear beam theory.

ABSTRACT

Stresses Due to Environmental Conditioning
of Cross-ply Graphite/Epoxy Laminates. (August 1979)
David Alan Douglass, B.S. A.& A.E., Purdue University:
Chairman of Advisory Committee: Dr. Y. Weitsman

This thesis concerns the internal residual stresses due to the environmental conditioning of cross-ply graphite/epoxy laminates, where moisture is induced into the material by exposure to high relative humidity at elevated temperatures.

The stress fields resulting from conditioning at two temperature levels are determined and compared for various symmetric cross-ply graphite/epoxy laminates by means of both elastic and viscoelastic analyses. The formulation considers temperature-dependent moisture diffusion and time, temperature and moisture dependent stress relaxation. The computations are based upon recent data and employ realistic values of material parameters.

The analysis shows that the viscoelastic stresses are much smaller than those predicted by elastic analysis, and that conditioning at 150°F results in residual stresses which are smaller than those reached during conditioning at 180°F.

ABSTRACT

Experimental Investigation of Moisture and Temperature Conditioning of C600/5208 Graphite/Epoxy Composite Material (December 1979)

Kenneth Allen Grieger, B.S.A.E., Purdue Univeristy;

Chairman of Advisory Committee: Dr. R. A. Schapery

There are three main questions to be investigated in this thesis. This first objective is to determine if a very high relative humidity (e.g. 98 percent) environment has approximately the same effect as the more easily conducted water soak condition on the moisture gain and damage level of the specimen. The second objective is to determine if the maximum moisture content at different relative humidities is independent of temperature. The third objective is to determine the amount of surface cracking for various environments.

An examination by means of a light microscope and water absorption rate of C600/5208 composite laminates, both crossply and unidirectional, which had been exposed to high temperature and moisture conditions is described. An attempt is made to explain these observations by means of surface cracks and physical properties.

The hygrothermal conditions which were used to condition the laminates were 98 percent relative humidity and water immersion each at room temperature and at 120°, 150°, 180° and 200°F. For each laminate orientation, comparisons are made between the effect of each of the temperatures and between the two moisture condtions. The coefficient of diffusion is calculated at each temperature from the moisture desorption curves of saturated specimens.

ABSTRACT

Determination of the Relationship of Free Volume to Mechanical Behavior for an Epoxy System Subjected to Various Aging Histories. (December 1979)

Darryl Steven Ring, B.S., Iowa State University

Chairman of Advisory Committee: Dr. W. L. Bradley

An epoxy resin commonly used in advanced composite materials for aerospace applications was tested for viscoelastic behavior after being aged under various cooling rates and steady state temperatures. In addition, the changes in free volume for the same aging conditions were studied. A discussion of the correlation between free volume and viscoelastic response is included. Data obtained from these experiments is useful in contributing to an overall understanding of factors important to the optimization of processing parameters in the manufacture of composite material components.

ABSTRACT

Aeroelastic Tailoring of Composite Materials (August 1979)

Jesse Byron Rogers, Jr., B.S., Mississippi State University;

M.S., University of Texas

Chairman of Advisory Committee: Dr. Walter J. Horn

The behavioral characteristics of lifting surface structures may be controlled through the utilization of properly tailored composite laminates. Variables such as the number of material systems used, the number of layers, the properties of the constituent fiber and matrix materials for each system employed, and the orientation and location of each ply in the laminate may be considered in the design process. The concept of controlling the structural response by optimizing these variables is called aeroelastic tailoring.

In this report, the type of structural response to applied loads for various composite laminates and the dependence of this response on the material parameters are illustrated. Previous investigations of aeroelastic tailoring are assessed and important areas requiring further research are identified and evaluated.

6. PROFESSIONAL PERSONNEL INFORMATION

6.1 Faculty Research Assignments

Each participating faculty member is responsible for the research conducted in at least one specific area of investigation, as shown below. In addition, most serve as chairmen of one or more of the graduate advisory committees for M.S. students and, as such, direct their students' research project. The faculty also contribute to other research activities on the project by serving on student advisory committees, through technical meetings, informal discussions, and, in some cases, through specific research work.

The Principal Investigator (R. A. Schapery) has responsibility for overall technical direction and coordination and for project management. In addition he has direct responsibility for certain research work, as noted below.

Faculty Member/Departmental Affiliation	Primary Research Responsibility
Dr. Richard Schapery/Aerospace and Civil Engineering	Principal Investigator and Theoretical Models for Physical Aging, Damage Growth, and Fracture.
Dr. Walter Bradley/Mechanical Engineering	Physical Aging Behavior, Delamination Fracture Properties.
Dr. Walter Haisler/Aerospace Engineering	Development of Finite Element Models.
Dr. Joe Ham/Physics	Curing and Aging Studies.
Mr. Bob Harbert/Civil Engineering	Duomorph Gage
Dr. Ken Jerina/Civil Engineering	Experimental Data Base, Mechanical and Failure Property Characterization.
Dr. John Randall/Nuclear Engineering	Neutron Radiography.
Dr. Jack Weitsman/Civil Engineering	Constitutive Relations, Environmental Effects.

6.2 Additional Professional Staff

Mechanics and Materials Research Center:

Mr. Carl Fredericksen - Electronics Technician

Mr. Mark McEndree - Research Assistant

Mr. William Eue - Computer Programmer

Nuclear Science Center:

Mr. Joseph Taft - Research Engineer

6.3 Spoken Papers and Lectures at Conferences and Other Professional Activities of the Faculty Related to Composite Materials (15 January 1979 - 31 December 1979):

R. A. Schapery

Conference Presentation:

"Analysis of Damage Growth and Failure for Viscoelastic Composite Materials", Society of Rheology Golden Jubilee Meeting, Boston, October 1979.

Workshops:

Participant in "Workshop on Damping in Composite Materials", MIT. Sponsored by AFFDL. April 1979.

Co-chairman of Polymer Science Division of "Workshop on Microstructure Mechanisms and Macromechanical Behavior of Materials", Cincinnatti, Ohio. Sponsored by NSF and AFOSR. May 1979.

Technical Committee Membership:

Member of the committee "High Temperature Metal and Cermaic Matrix Composites", National Materials Advisory Board, Washington, D.C. Sponsored by DOD. 1979-1980.

W. L. Bradley

Conference Presentations:

Gordon conference lecture on research in progress in the area of physical aging of epoxy resin, Santa Barbara, California. January 1979.

"Fracture Toughness Studies of Cast Iron using a J-integral Approach", Third International Conference on Mechanical Behavior of Materials, Cambridge, England. August 1979.

Technical Committee Membership:

Member of committee ASTM E-24 on fracture.

Member of Metal Properties Council, sponsored jointly by ASME, ASM and ASTM.

W. E. Haisler

Conference Presentation:

"An Incremental Form of the Single-Integral Nonlinear Viscoelastic Theory for Elastic-Plastic-Creep Finite Element Analysis," *ASME Pressure Vessels and Piping Conference*, San Francisco, Calif. June 1979.

K. L. Jerina

Technical Committee Membership:

Member and Corresponding Secretary for ASTM Committee E-9 on Fatigue.

Member of the SAE Committee on Fatigue Design and Evaluation and Chairman of the Task Force on Composite Materials:

May 1979: Organized and chaired a technical session on manufacturing technology for automotive composites.

Oct. 1979: Organized and chaired a technical session on fatigue and design of automotive composites.

Y. Weitsman

Conference Presentation:

"Residual Stresses due to Cool-Down of Epoxy Resin Composites", ASME Winter Meeting, N.Y. December 1979.

In addition to the above activities, the faculty attended several conferences on composites, lectured at various Universities and Industries and worked as consultants to industry in the composites area.

7. REFERENCES

1. Renton, W.J. and Ho, T., "The Effect of Envoronment on the Mechanical Response of AS/3501-6 Graphite/Epoxy Material", Vought Corp. Advanced Technology Center Final Report, Aug. 1978. Contract No. N00019-77-C-0369 with the Department of the Navy.

2. Williams, M.L., et al., "Mechanical Spectroscopy for Epoxy Resins", Interim Technical Report, Sept. 1977 - March 1979, Univ. of Pittsburgh, Contract No. F33615-77-C-5232 with AFML.

3. Struik, L.C.E., Physical Aging in Amorphous Polymers and Other Materials, Elsevier (1978).

4. Weitsman, Y., "Residual Thermal Stresses due to Cool-Down of Epoxy-Resin Composites". J. Applied Mechanics, ASME Vol. 46, No. 3, pp. 563-567, Sept. 1979.

5. Briar, H.P., Bills, K.W. Jr., and Schapery, R.A., "Design and Test of the Operational In-Situ Gage for Solid Propellant Surveillance," Final Report, Air Force Rocket Propulsion Laboratory Report No. AFRPL-TR-76-36 (Contract No. F04611-73-C-0040) June 1976.

6. Haisler, W.E., "AGGIE I - A Finite Element Program for Nonlinear Structural Analysis," TEES Report 3275-77-1, Aerospace Engineering Department, Texas A&M University, June 1977.

7. Sanders, D.R. and Haisler, W.E., "An Incremental Form of the Single-Integral Nonlinear Viscoelastic Theory for Elastic-Plastic-Creep Finite Element Analysis", Paper 79-PVP-114, ASME PVP Conference, San Francisco, March 1979.

APPENDIX A

Recently Completed Reports and Publications

1. "Interfacial Stresses in Viscoelastic Adhesive-Layers Due to Moisture Sorption" by Y. Weitsman.

2. "Residual Thermal Stresses Due to Cool-Down of Epoxy-Resin Composites" by Y. Weitsman.

3. "Optimal Cool-Down in Linear Viscoelasticity" by Y. Weitsman.

4. "Residual Stresses due to Environmental Conditioning of Cross-Ply Graphite/Epoxy Laminates" by Y. Weitsman.

5. "Thermal Buckling of Free Plates due to Non-Uniform Temperature Distribution" by Y. Weitsman.

6. "A Method For Determining the Mode I Delamination Fracture Toughness of Elastic and Viscoelastic Composite Materials" by D.F. Devitt, R.A. Schapery, and W.L. Bradley.

Int. J. Solids Structures Vol. 15, pp. 701–713
Pergamon Press Ltd., 1979. Printed in Great Britain

INTERFACIAL STRESSES IN VISCOELASTIC ADHESIVE-LAYERS DUE TO MOISTURE SORPTION

Y. WEITSMAN
Mechanics and Materials Research Center, Texas A&M University, College Station, TX 77843, U.S.A.

(*Received* 30 *August* 1978; *revised* 15 *December* 1978)

Abstract—This paper concerns the mechanical behavior of an epoxy adhesive layer that is located between stiff adherends as the adhesive absorbs moisture from the ambient environment.

As the moisture penetrates the layer by an extremely slow diffusion process the eposy undergoes a simultaneous process of stress-relaxation. Calculations of viscoelastic interfacial stresses were performed for a time-dependent response which is typical of epoxy for a layer geometry as encountered in practice.

The results show that for exposure to steady ambient humidity the viscoelastic stresses are smaller than their elastic counterparts. However, under fluctuating ambient humidity the viscoelastic response may cause stress reversals, and thereby failure modes, which are not predicted by elasticity theory.

1. INTRODUCTION

Adhesive bonding forms an attractive method of joining structural members. In analyzing the stresses which develop within the bond it is necessary to account for the fact that the adhesive materials respond in a viscoelastic manner under loads and their time-dependent behavior is greatly affected by moisture and temperature.

When two adherends are joined together by a thin adhesive layer the adhesive absorbs moisture from the ambient environment, at its exposed edges, which induces swelling strains into the layer. Since the adherends are much stiffer than the adhesive they constrain the adhesive-layer against its tendency to swell, thus causing the formation of extremely high stresses within the layer. In this paper attention is focused on the interfacial-stresses which arise at the interfaces between the adherends and the adhesive.

Since the moisture penetrates the layer by an extremely slow diffusion process, the epoxy may undergo noticeable creep and relaxation while the diffusion process is in progress. The main purpose of this paper is to relate the interaction, which occurs concurrently, between the two time-dependent phenomena—moisture-diffusion and stress-relaxation.

The analysis employs a variational method and is inherently approximate in nature. It is due to this approximation that the edge singularity in the stress field is replaced here by finite, though large, values. However, for the exceedingly thin layers that are utilized in practice, the selected expressions for the displacement fields should provide a good approximation. Furthermore, the approximation should not detract from the basic purpose of this work which is to provide information about the relative influence of the diffusion and relaxation times.

2. FORMULATION

Consider a semi-infinite, isotropic and elastic adhesive layer, of thickness $2a$, between two semi-infinite adherend plates as shown in Fig. 1.

Let X, Y denote Cartesian coordinates and t time. Let $\varepsilon(X, t)$ represent the unconstrained swelling induced by moisture and μ, ν be the elastic-shear-modulus and Poisson's ratio, respectively. Assume a state of plane-strain.

Introduce the following non-dimensional quantities

$$x = X/a,\ y = Y/a,\ e(x, t) = \varepsilon(X/a, t)$$
$$s_x = \sigma_x/\mu,\ s_y = \sigma_y\ \mu,\ s_{xy} = \tau_{xy}/\mu. \tag{1}$$

Also, denote

$$f_1 = 2\nu/(1-2\nu),\quad f_2 = 2(1-\nu)/(1-2\nu),\quad f_3 = 2(1+\nu)/(1-2\nu).$$

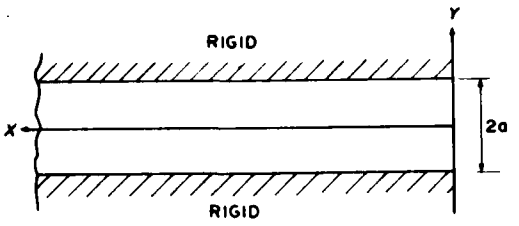

Fig. 1. The adhesive layer between rigid adherends exposed to moisture at $X = 0$.

Consider now the following, approximate, form for the displacement fields within the adhesive-layer

$$U(X, Y) = a u_0(x) + \frac{1}{2} a\, u_2(x) y^2$$
$$V(X, Y) = a\, v_1(x) y + \frac{1}{3} a\, v_3(x) y^3. \tag{2}$$

In (2) U and V are components of displacement in the X and Y directions, respectively, and u_0, u_2, v_1, v_3 are dimensionless, yet to be determined functions of the dimensionless coordinate x. Note that for an induced swelling-strain of the form $e(x, t)$ the displacements U and V possess the required symmetries in Y.

Form (2) is the lowest-order approximation which provides information on the interfacial stresses, at the boundary between adhesive and adherend, in a self-contained manner. For exceedingly thin layers the approximation should provide sufficient accuracy.

Expressions (2) are essentially the same as used in Ref. [1].

Employing Hooke's law we obtain the following non-dimensional form for stress–strain relations:

$$\begin{bmatrix} s_x \\ s_y \\ s_{xy} \end{bmatrix} = \begin{bmatrix} f_2 & f_1 & f_3 & 0 \\ f_1 & f_2 & f_3 & 0 \\ 0 & 0 & 0 & 1 \end{bmatrix} \begin{bmatrix} u_0' + \frac{1}{2} u_2' y^2 \\ v_1 + v_3 y^2 \\ -e \\ u_2 y + v_1' y + \frac{1}{3} v_3' y^3 \end{bmatrix} \tag{3}$$

where primes designate derivatives with respect to x.

In addition, due to the assumed rigidity and immobility of the adherends we have the following boundary conditions:

$$u(x, 1, t) = 0$$
$$v(x, 1, t) = 0. \tag{4}$$

In view of the constraints implied by boundary conditions (4) it is obvious that, when employing a variational formulation, the unknown functions u_0, u_2, v_1, and v_3 in (2) cannot be varied independently. As noted in [1] the four above mentioned functions can be treated independently of each other by introducing suitable Lagrange multipliers s_n and s_t. It turns out that s_n and s_t, which are the dimensionless force-conjugates of $v(x, 1, t)$ and $u(x, 1, t)$ respectively, represent the sought after interfacial normal and shear stresses.

Employment of the principle of virtual work, and utilization of the Lagrange multipliers in analogy with [1],† yields the following expression for the variation of the internal energy δE

†See particularly the section Variational Formulation of the Totally Constrained Case ($v_0 = 0$).

$$\delta E = \mu a^2 \int_0^\infty \left\{ \int_0^1 \left[s_x \left(\delta u_o' + \frac{1}{2} y^2 \delta u_2' \right) + s_y (\delta v_1 + y^2 \delta v_3) + s_{xy} \left(y \delta u_2 + y \delta v_1' + \frac{1}{3} y^3 \delta v_3' \right) \right] dy \right.$$

$$\left. - s_t \left(\delta u_0 + \frac{1}{2} \delta u_2 \right) - \delta s_t \left(u_0 + \frac{1}{2} u_2 \right) - s_n \left(\delta v_1 + \frac{1}{3} \delta v_3 \right) - \delta s_n \left(v_1 + \frac{1}{3} v_3 \right) \right\} dx. \quad (5)$$

Similarly, the variation of the external work, δW, is given by

$$\delta W = \mu a^2 \int_0^1 \left[s_x^*(0, y) \left(\delta u_0 + \frac{1}{2} y^2 \delta u_2 \right) + s_{xy}^*(0, y) \left(y \delta v_1 + \frac{1}{3} y^3 \delta v_3 \right) \right] dy. \quad (6)$$

Integration by parts of (5) and employment of (3) yield, upon factoring out the now independent variations δu_0, δu_2, δv_1 and δv_3:

$$\begin{aligned}
&\frac{2}{3} f_2 u_0'' - f_3 e' + s_t = 0 \\
&\frac{1}{15} f_2 u_0'' - \frac{2}{15} (f_1 + 1) v_1' + \frac{2}{3} u_0 - \frac{1}{6} f_3 e' + \frac{1}{2} s_t = 0 \\
&\frac{2}{3} (f_1 + 1) u_0' - \frac{2}{15} v_1'' - f_3 e - s_n = 0 \\
&\frac{2}{5} (f_1 + 1) u_0' - \frac{2}{35} v_1'' - \frac{4}{5} f_2 v_1 - f_3 e - s_n = 0.
\end{aligned} \quad (7)$$

To these are adjoined the constraint conditions

$$\begin{aligned}
&u_0 + \frac{1}{2} u_2 = 0 \\
&v_1 + \frac{1}{3} v_3 = 0.
\end{aligned} \quad (8)$$

Equations (7) and (8) express the field equations of the problem. The concomitant from the integration-by-parts of (5) combines with (6) to determine the boundary conditions at $x = 0$. This combination, together with (3), yields

$$\begin{aligned}
&-7 u_0 + 2 v_1' = 0 \\
&2 u_0' + \frac{f_1}{f_2} v_1 = \frac{5}{2} \frac{f_3}{f_2} e(0, t).
\end{aligned} \quad (9)$$

Note that the boundary conditions (9) were obtained after employment of (8), which hold also at $x = 0$.

In order to solve for u_0 and v_1 we first eliminate s_t between the first pair of (7) and s_n between the last pair. Next, we employ (8) to eliminate u_2 and v_3. This procedure yields:

$$\begin{aligned}
&2 f_2 u_0'' + (f_1 + 1) v_1' - 5 u_0 = \frac{5}{2} f_3 e' \\
&\frac{2}{7} v_1'' - (f_1 + 1) v_0' - 3 f_2 v_1 = 0.
\end{aligned} \quad (10)$$

The solution of (10) is expressed with the aid of the following second order equation

$$\frac{4}{7} f_2 Z^2 + \left[(f_1 + 1)^2 - 6 f_2^2 - \frac{10}{7} \right] Z + 15 f_2 = 0. \quad (11)$$

Denote the roots of (11) by Z_1 and Z_2 and define

$$\alpha_1 = \sqrt{Z_1}, \quad \alpha_2 = \sqrt{Z_2}$$

$$\chi_{1,2} = \frac{(f_1+1)\alpha_{1,2}}{(2f_1)Z_{1,2} - 3f_2} \qquad D = \frac{5}{4}\frac{f_3}{f_2}\frac{1}{\alpha_1\chi_2 - \alpha_2\chi_1}.$$

The solution of (10), which vanishes as $x \to \infty$, is

$$u_0 = D\left[\chi_1\int_x^\infty \sinh\alpha_2(x-s)e'(s)\,ds - \chi_2\int_x^\infty \sinh\alpha_1(x-s)e'(s)\,ds\right] + A_1 e^{-\alpha_1 x} + A_2 e^{-\alpha_2 x}$$

$$v_1 = D\chi_1\chi_2\int_x^\infty \left[\cosh\alpha_2(x-s) - \cosh\alpha_1(x-s)\right]e'(s)\,ds - \chi_1 A_1 e^{-\alpha_1 x} - \chi_2 A_2 e^{-\alpha_2 x}. \tag{12}$$

In (12) A_1 and A_2 are arbitrary constants that are determined with the aid of boundary conditions (9).

3. ELASTIC SOLUTION FOR MOISTURE DIFFUSION UNDER CONSTANT AMBIENT HUMIDITY

It has been observed [2], [3]† that the saturation-moisture level in "neat" epoxy, as well as in epoxy-based composites, depends on the relative humidity of the ambient environment. The dilatational strains that accompany moisture sorption are about 2/3 of the swelling that would be anticipated by straightforward "volume additivity".

The penetration of moistures into several epoxy resins was shown to follow the classical diffusion equations [2–4].

For the one-dimensional diffusion process considered herein, it follows that under constant ambient humidity the moisture-induced swelling is given by

$$\epsilon(X,t) = A\,\mathrm{erfc}\left(\frac{X}{2\sqrt{kt}}\right). \tag{13}$$

In (13) A is a constant which converts moisture content to dilatational strain and k is the coefficient of moisture diffusion.

Introduce the non-dimensional time $\beta = kt/a^2$, then the non-dimensional version of (13) reads

$$e(x,\beta) = A\,\mathrm{erfc}(x/2\sqrt{\beta}). \tag{14}$$

Substitution of (14) into (12) leads to a closed-form solution for all the integrals therein [5, 6], e.g.

$$\int_x^\infty \sinh\alpha(x-s)e'(s)\,ds = -\frac{A}{2}e^{\beta\alpha^2}\left\{\sinh\alpha x\left[1 - \frac{1}{2}\left(\mathrm{erf}\left(\frac{x}{2\sqrt{\beta}} + \alpha\sqrt{\beta}\right)\right.\right.\right.$$

$$\left.\left.\left. - \mathrm{erf}\left(\frac{x}{2\sqrt{\beta}} - \alpha\sqrt{\beta}\right)\right)\right] - \frac{1}{2}\cosh\alpha x\left[\mathrm{erf}\left(\frac{x}{2\sqrt{\beta}} + \alpha\sqrt{\beta}\right) - \mathrm{erf}\left(\frac{x}{2\sqrt{\beta}} - \alpha\sqrt{\beta}\right)\right]\right\}$$

and a similar expression for

$$\int_x^\infty \cosh\alpha(x-s)e'(s)\,ds.$$

With the simpler, closed-form version of u_0 and v_1 that replaces all the integrals in (12) it is possible to evaluate analytically the unknowns A_1 and A_2 therein.

†For most of this information, the author is greatly indebted to Messrs. J. E. Halkias and E. L. McKague of General Dynamics Corporation, Fort Worth Division.

Employing the boundary conditions (9), with $e(0, t) = A$, the values of A_1 and A_2 are determined from the following two-by-two algebraic system:

$$\begin{bmatrix} L_1 & L_2 \\ M_1 & M_2 \end{bmatrix} \begin{bmatrix} A_1 \\ A_2 \end{bmatrix} = \begin{bmatrix} D(-L_2\chi_1 J_2 + L_1\chi_2 J_1) \\ -\frac{5}{2}\frac{f_3}{f_2}A + D(-M_1\chi_2 K_1 + M_2\chi_1 K_2) \end{bmatrix} \tag{15}$$

where, in (15)

$$L_{1,2} = 7 - (2\alpha\chi)_{1,2} \qquad M_{1,2} = \left(2\alpha + \frac{f_1}{f_2}\chi\right)_{1,2}$$

$$K_{1,2} = -A\, e^{\beta\alpha_{1,2}^2} \qquad J_{1,2} = -K_{1,2}\,\mathrm{erf}(\alpha_{1,2}\sqrt{\beta}).$$

Solving for A_1 and A_2 from (15) we obtain the complete solution to u_0 and v_1 in (12). This, in turn, enables us to evaluate the interfacial tractions s_n and s_t by using the first and third of eqns (7).

After straightforward, though tedious, manipulations we obtain

$$\begin{aligned} s_n(x,\beta) &= \frac{2}{3}D\,[\alpha_2\chi_1 P_2 K_2(x,\beta) - \alpha_1\chi_2 P_1 K_1(x,\beta)] \\ &\quad -\frac{2}{3}\alpha_1 P_1 A_1\, e^{-\alpha_1 x} - \frac{2}{3}\alpha_2 P_2 A_2\, e^{-\alpha_2 x} - f_3\, e(x,\beta) \\ s_t(x,\beta) &= -\frac{2}{3}f_2 D[\alpha_2^2\chi_1 J_2(x,\beta) - \alpha_1^2\chi_2 J_1(x,\beta)] \\ &\quad -\frac{2}{3}f_2(\alpha_1^2 A_1\, e^{-\alpha_1 x} + \alpha_2^2 A_2\, e^{-\alpha_2 x}) - \frac{Af_3}{6\sqrt{\pi\beta}}\, e^{-(x^2/4\beta)}. \end{aligned} \tag{16}$$

In (16)

$$J_{1,2}(x,\beta) = -\frac{A}{2}\, e^{\beta\alpha_{1,2}^2}(\psi_{1,2}^{+} - \psi_{1,2}^{-})$$

$$K_{1,2}(x,\beta) = -\frac{A}{2}\, e^{\beta\alpha_{1,2}^2}(\psi_{1,2}^{+} + \psi_{1,2}^{-})$$

where

$$\psi_{1,2}^{+} = e^{\alpha_{1,2}x}\,\mathrm{erfc}(\alpha_{1,2}\sqrt{\beta} + x/2\sqrt{\beta})$$

$$\psi_{1,2}^{-} = e^{-\alpha_{1,2}x}\,\mathrm{erfc}\,(-\alpha_{1,2}\sqrt{\beta} + x/2\sqrt{\beta}).$$

Also,

$$P_{1,2} = f_1 + 1 - \frac{1}{5}(\alpha\chi)_{1,2}.$$

Form (16) is the elastic solution to the present problem. While this form provides a necessary step toward the generation of the viscoelastic solution, because its Laplace transform is readily available, it cannot be evaluated numerically for a wide range of x and t because $J_1(x, \beta)$, $K_1(x, \beta)$, A_1 and A_2 become numerically unstable.† Difficulties of this sort stem from the peculiar geometry of the adhesive layer, namely, the extremely small ratio of thickness to length.

†For $x = 3$ and $t = 1000$, with typical values for k, a and v, J_1 and K_1 involve products of numbers of $O(10^{22})$ with numbers of $O(10^{-22})$, thus exceeding the accuracy provided even by "double precision".

The difficulty is overcome by the employment of an approximate form of erfc (z), as follows[7]:

$$\operatorname{erfc} z = Q(t(z))\, e^{-z^2}$$

where (17)

$$Q(t) = \sum_{j=1}^{5} a_j t^j \text{ and } t(z) = (1+pz)^{-1}\ddagger.$$

Appropriate substitution of (17) into (16) yields an alternative, numerically stable, form for the interfacial stresses. We obtain

$$\begin{aligned}
\frac{1}{A}s_n(x,\beta) &= \frac{5}{3}\frac{f_3}{f_2}\frac{\alpha_2 P_2 L_1 e^{-\alpha_2 x} - \alpha_1 P_1 L_2 e^{-\alpha_1 x}}{\Delta} - f_3 \operatorname{erfc}(x/2\sqrt{\beta}) \\
&+\frac{2}{3}D\Big\{-\alpha_2\chi_1 P_2\Big[\frac{1}{2}e^{(x^2/4\beta)}\Big(Q\Big(\alpha_2\sqrt{\beta}+\frac{x}{2\sqrt{\beta}}\Big)+h(x-2\alpha_2\beta)Q\Big(\Big|\alpha_2\sqrt{\beta}-\frac{x}{2\sqrt{\beta}}\Big|\Big)\Big) \\
&- H(x-2\alpha_2\beta)\, e^{\beta\alpha_2^2-\alpha_2 x}\Big] + \alpha_1\chi_2 P_1\Big[\frac{1}{2}e^{-(x^2/4\beta)}\Big(Q\Big(\alpha_1\sqrt{\beta}+\frac{x}{2\sqrt{\beta}}\Big) \\
&+ h(x-2\alpha_1\beta)Q\Big(\Big|\alpha_1\sqrt{\beta}-\frac{x}{2\sqrt{\beta}}\Big|\Big)\Big) - H(x-2\alpha_1\beta)\, e^{\beta\alpha_1^2-\alpha_1 x}\Big] \\
&+\frac{B}{\Delta}\Big(\alpha_1 P_1 M_2 e^{-\alpha_1 x} - \alpha_2 P_2 M_1 e^{-\alpha_2 x}\Big)\Big\}
\end{aligned}$$

$$\begin{aligned}
\frac{1}{A}s_t(x,\beta) &= \frac{5}{3}\frac{f_3}{\Delta}\Big(\alpha_2^2 L_1 e^{-\alpha_2 x} - \alpha_1^2 L_2 e^{-\alpha_1 x}\Big) - \frac{1}{6}\frac{f_3}{\sqrt{\pi\beta}}e^{-(x^2/4\beta)} \\
&+\frac{2}{3}f_2 D\Big\{\alpha_2^2\chi_1\Big[\frac{1}{2}e^{-(x^2/4\beta)}\Big(Q\Big(\alpha_2\sqrt{\beta}+\frac{x}{2\sqrt{\beta}}\Big)-h(x-2\alpha_2\beta)Q\Big(\Big|\alpha_2\sqrt{\beta}-\frac{x}{2\sqrt{\beta}}\Big|\Big)\Big) \\
&+ H(x-2\alpha_2\beta)\, e^{\beta\alpha_2^2-\alpha_2 x}\Big] - \alpha_1^2\chi_2\Big[\frac{1}{2}e^{-(x^2/4\beta)}\Big(Q\Big(\alpha_1\sqrt{\beta}+\frac{x}{2\sqrt{\beta}}\Big) \\
&- h(x-2\alpha_1\beta)Q\Big(\Big|\alpha_1\sqrt{\beta}-\frac{x}{2\sqrt{\beta}}\Big|\Big)\Big) + H(x-2\alpha_1\beta)\, e^{\beta\alpha_1^2-\alpha_1 x}\Big] \\
&+\frac{B}{\Delta}\Big(\alpha_1^2 M_2 e^{-\alpha_1 x} - \alpha_2^2 M_1 e^{-\alpha_2 x}\Big)\Big\}.
\end{aligned} \tag{18}$$

In (18)

$$H(\xi) = \begin{cases} 0 & \xi < 0 \\ 1 & \xi \geq 0 \end{cases} \qquad h(\xi) = \begin{cases} -1 & \xi < 0 \\ 1 & \xi > 0 \end{cases}$$

and

$$\Delta = L_1 M_2 - L_2 M_1, \quad B = \chi_2 L_1 Q(\alpha_1\sqrt{\beta}) - \chi_1 L_2 Q(\alpha_2\sqrt{\beta}).$$

As $t \to \infty$ the "fully saturated" elastic solution, obtained by taking limits of (18) as $\beta \to \infty$, reads

$$\begin{aligned}
\frac{1}{A}s_n(x,\infty) &= -f_3\Big[1+\frac{5}{3}\frac{1}{f_2\Delta}(\alpha_1 P_1 L_2 e^{-\alpha_1 x} - \alpha_2 P_2 L_1 e^{-\alpha_2 x})\Big] \\
\frac{1}{A}s_t(x,\infty) &= -\frac{5}{3}\frac{f_3}{\Delta}(\alpha_1^2 L_2 e^{-\alpha_1 x} - \alpha_2^2 L_1 e^{-\alpha_2 x}).
\end{aligned} \tag{19}$$

‡The numerical value of a_j $(j = 1, 2, \ldots 5)$ and p are given in Section 7.1.26, on page 299 of Ref.[7]. This approximation is valid for all z.

4. VISCOELASTIC SOLUTION FOR MOISTURE DIFFUSION UNDER CONSTANT AMBIENT HUMIDITY

Uniaxial-tension experiments[8] on epoxy indicate that its creep-response can be described by a "power law" form as follows:

$$D(t;T) = D_0(T) + D_1\left[\frac{t}{a(T)}\right]^q. \tag{20}$$

In (20) T denotes temperature and $a(T)$ is the "shift-factor" function. Additional data on polyester[9] and epoxy[10] indicate that the creep-response depends also on the moisture content m, namely $D = D(t;T,m)$. However, this dependence is omitted in the present analysis. Furthermore, we shall consider the case of uniform temperature for the entire adhesive.

In most adhesives the Poisson's ratio ν remains constant under a wide range of conditions. Consequently we shall consider a viscoelastic shear-compliance of the form

$$\mu(t) = d_0(1 + d_1 t^q)$$

where

$$d_0 = 2(1+\nu)\,D_0.\dagger \tag{21}$$

Denote $\tau = a^2/k$ and $\tau_r = d_1^{-1/q}$. Let p be the variable of the Laplace transform in the time domain and $\eta = p\tau$. Finally, let the ratio between the characteristic diffusion time τ and the characteristic creep time τ_r be $\theta = \tau_r/\tau$.

Then, the Laplace-transform of (21) is

$$\frac{1}{d_0}p\bar{D}(p) = 1 + \frac{\Gamma(q+1)}{(\theta\eta)^q}. \tag{22}$$

The reciprocity relations between the transforms of the creep and relaxation functions[11] yield

$$d_0 p\bar{E}(p) = 1/[1 + \Gamma(q+1)/(\theta\eta)^q] = R(\theta\eta). \tag{23}$$

Upon insertion of the explicit expressions for A_1 and A_2 into (16), the Laplace transforms of the elastic stresses (denoted by $\hat{s}$) become

$$\begin{aligned}
\frac{1}{A}p\hat{s}_n(x,p) = \frac{2}{3}D\Bigg[&\eta\left(\frac{\alpha_1\chi_2P_1}{\sqrt{\eta}+\alpha_1}\cdot\frac{e^{-\sqrt{\eta}x}-e^{-\alpha_1x}}{\sqrt{\eta}-\alpha_1} - \frac{\alpha_2\chi_1P_2}{\sqrt{\eta}+\alpha_2}\cdot\frac{e^{-\sqrt{\eta}x}-e^{-\alpha_2x}}{\sqrt{\eta}-\alpha_2}\right)\\
&+\sqrt{\eta}\left(\frac{\chi_2L_1}{\sqrt{\eta}+\alpha_1} - \frac{\chi_1L_2}{\sqrt{\eta}+\alpha_2}\right)\frac{\alpha_1P_1M_2e^{-\alpha_1x} - \alpha_2P_2M_1e^{-\alpha_2x}}{\Delta}\Bigg]\\
&- f_3e^{-\sqrt{\eta}x} + \frac{5}{3}\frac{f_3}{f_2}\frac{\alpha_2P_2L_1e^{-\alpha_2x} - \alpha_1P_1L_2e^{-\alpha_1x}}{\Delta}\\
\frac{1}{A}p\hat{s}_t(x,p) = &-\frac{f_3}{6}\sqrt{\eta}\,e^{-\sqrt{\eta}x} - \frac{5}{3}f_3\frac{L_2\alpha_1^2e^{-\alpha_1x} - L_1\alpha_2^2e^{-\alpha_2x}}{\Delta}\\
&-\frac{2}{3}f_2D\sqrt{\eta}\Bigg[\frac{\alpha_1^2\chi_2}{\sqrt{\eta}+\alpha_1}\frac{\sqrt{\eta}\,e^{-\alpha_1x} - \alpha_1e^{-\sqrt{\eta}x}}{\sqrt{\eta}-\alpha_1} - \frac{\alpha_2^2\chi_1}{\sqrt{\eta}+\alpha_2}\frac{\sqrt{\eta}\,e^{-\alpha_2x} - \alpha_2e^{-\sqrt{\eta}x}}{\sqrt{\eta}-\alpha_2}\\
&+\left(\frac{\chi_2L_1}{\sqrt{\eta}+\alpha_1} - \frac{\chi_1L_2}{\sqrt{\eta}+\alpha_2}\right)\frac{\alpha_2^2M_1e^{-\alpha_2x} - \alpha_1^2M_2e^{-\alpha_1x}}{\Delta}\Bigg].
\end{aligned} \tag{24}$$

Note that the singularities at $\sqrt{\eta} = \alpha_1$ and $\sqrt{\eta} = \alpha_2$ are removable.

†The non-dimensional viscoelastic stresses are given by $s_{ij} = \sigma_{ij}/d_0$.

From the fundamental equations of linear viscoelasticity[12] it follows that the Laplace transforms of the viscoelastic solution to our problem (denoted by overbars) are

$$\frac{d_0}{A} p\bar{s}_n(x, p) = R(\theta\eta) \cdot \frac{1}{A} p\hat{s}_n(x, p)$$
$$\frac{d_0}{A} p\bar{s}_t(x, p) = R(\theta\eta) \cdot \frac{1}{A} p\hat{s}_t(x, p). \tag{25}$$

In order to obtain the viscoelastic solution in the real-time domain it is necessary to invert (25). The inversion was obtained by the method of collocation[13]. Typically, expressions (25) were plotted vs $\log \eta$ and a set on N points $\eta_i (i = 1, \ldots N)$ was selected to cover the ranges where those plots show noticeable curvatures. It was found that the shapes of the above mentioned plots, as well as the locations of high curvature regions, depended on x. Therefore, it was impossible to employ any specific set of points η_i in the inversion and an appropriate selection had to be made for each value of x.

The calculations followed the scheme of Ref.[13]. Note, however, that for a "power-law" creep as given in (20) we have $\lim_{t\to\infty} D(t, T) \to \infty$, hence the equilibrium stress vanishes. Furthermore, in the present case the transform-variable is $\eta = p\tau$, whereby the inversion is obtained in terms of dimensionless time t/τ, rather than real time t.

Calculations were performed for an adhesive-layer with the following selected properties:

Thickness $a = 0.003''$, moisture diffusivity $k = 0.2 \times 10^{-8}$ in^2/sec, Poisson's ratio $\nu = 0.45$, 100% R. H.-to-swelling conversion-factor $A = 0.03$, creep compliances $D_0 = 2 \times 10^{-6}$ in^2/lb, $D_1 = 0.2 \times 10^{-6}$ in^2/lb with $q = 0.19$. The corresponding value of the shift-factor function was $a(T) = 1$.

With the above numerical values we obtain $\tau = 4500\,\text{sec}^{-1}$ and the value of θ in (22) is $\theta = 2450$.

Numerical evaluations were performed on an Amdahl 470 digital computer. The results are shown in Figs. 2–9. The heavy solid lines in Figs. 2–7 show the dependence of the non-dimensional viscoelastic normal and tangential interlaminar stresses s_n and s_t on time t at three fixed stations within the layer, $x = X/a = 0.01$, 1 and 3, when the free edge ($x = 0$) is exposed to a constant R.H. = 100% at $t = 0$. Note that the time scale is logarithmic.

For comparison purposes, the elastic stresses—as given in (18)—are shown in thin solid lines in Figs. 2–7. Note that any station within the layer senses the build-up and approach of the

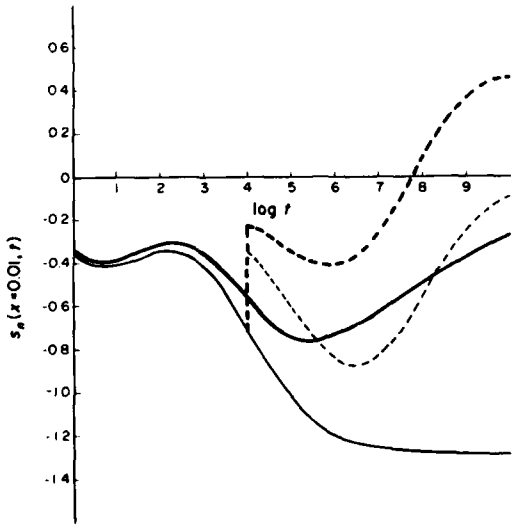

Fig. 2. Elastic and viscoelastic values of the non-dimensional normal interlaminar traction s_n at $x = X/a = 0.01$ vs. $\log t$ (t in seconds). Heavy lines—viscoelastic, thin lines—elastic. Solid lines—exposure to a constant ambient R.H., dashed lines—exposure to fluctuating ambient R.H. (according to eqn 29).

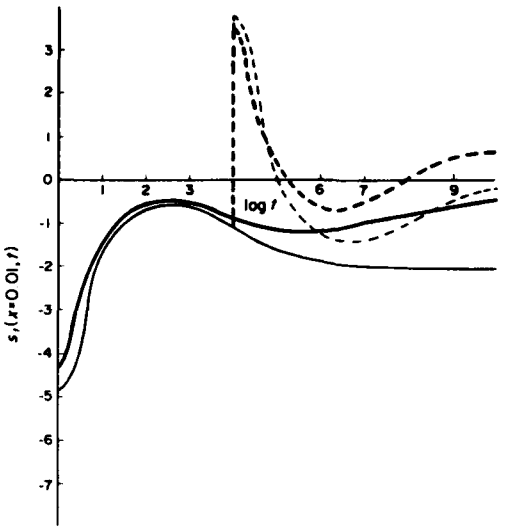

Fig. 3. Elastic and viscoelastic values of the non-dimensional tangential interlaminar traction s_t at $x = X/a = 0.01$ vs. log t (t in seconds). Heavy lines—viscoelastic, thin lines—elastic. Solid lines—exposure to a constant ambient R.H., dashed lines—exposure to fluctuating ambient R.H. (according to eqn 29).

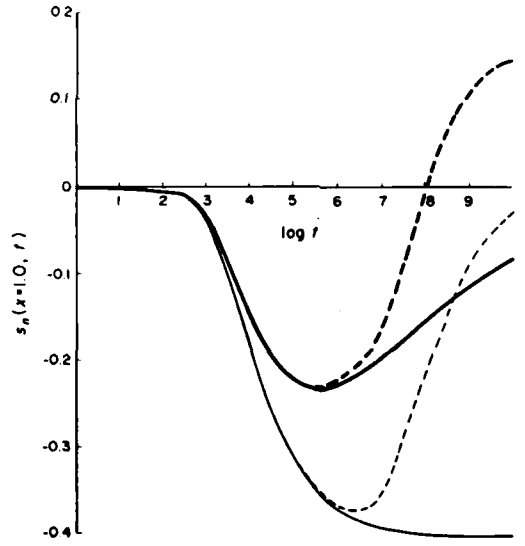

Fig. 4. Elastic and viscoelastic values of the non-dimensional normal interlaminar traction s_n at $x = X/a = 1$ vs log t (t in seconds). Heavy lines—viscoelastic, thin lines—elastic. Solid lines—exposure to a constant ambient R.H., dashed lines—exposure to fluctuating ambient R.H. (according to eqn 29).

moisture in a gradual manner and that a steep increase in stress occurs after the passage of a time-span, which depends on the characteristic diffusion time and the location of the station. Beyond that time the station notices a "fully saturated" state, which explains the leveling-off of the elastic stresses for longer times.

The viscoelastic values, which are affected by relaxation, diminish to zero with time.

Thus far all viscoelastic results were obtained from inversion of (25) by means of collocation.

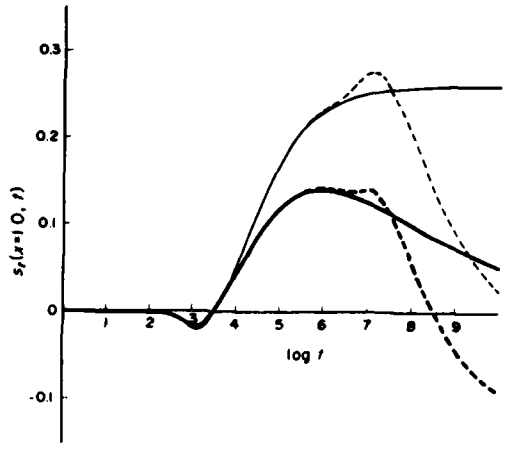

Fig. 5. Elastic and viscoelastic values of the non-dimensional tangential interlaminar traction s_t at $x = X/a = 1$ vs $\log t$ (t in seconds). Heavy lines—viscoelastic, thin lines—elastic. Solid lines—exposure to a constant ambient R.H., dashed lines—exposure to fluctuating ambient R.H. (according eo eqn 29).

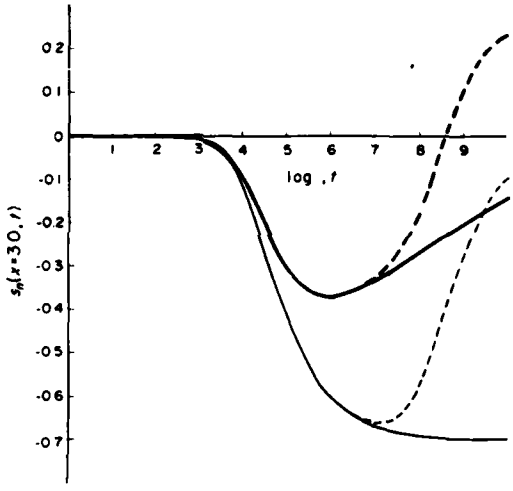

Fig. 6. Elastic and viscoelastic values of the non-dimensional normal interlaminar traction s_n at $x = X/a = 3$ vs $\log t$ (t in seconds). Heavy lines—viscoelastic, thin lines—elastic. Solid lines—exposure to a constant ambient R.H., dashed lines—exposure to fluctuating ambient R.H. (according to eqn 29).

Consider now an approximate expression for the relaxation modulus[14]

$$E(t) = \frac{1}{D(t)} \frac{\sin \pi n}{\pi n} \tag{26}$$

where

$$n = n(t) = \frac{d}{d \log t} D(t).$$

Employing (26), the "quasi-elastic" (viscoelastic) solution is given by[13]

$$\begin{aligned} s_n^{q.e.}(x, t) &= F(t) s_n(x, t) \\ s_t^{q.e.}(x, t) &= F(t) s_t(x, t) \end{aligned} \tag{27}$$

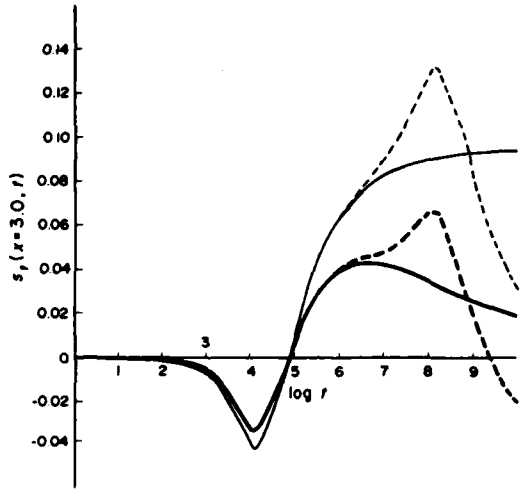

Fig. 7. Elastic and viscoelastic values of the non-dimensional tangential interlaminar traction s_t at $x = X/a = 3$ vs $\log t$ (t in seconds). Heavy lines—viscoelastic, thin lines—elastic. Solid lines—exposure to a constant ambient R.H., dashed lines—exposure to fluctuating ambient R.H. (according to eqn 29).

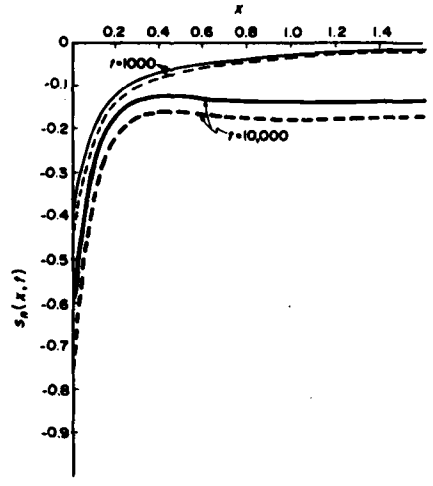

Fig. 8. Elastic and viscoelastic values of the non-dimensional normal interlaminar traction s_n at times $t = 1000$ sec and $t = 10{,}000$ sec vs x. Dashed lines—elastic, solid lines—viscoelastic.

where, in (27), $s_n(x, t)$ and $s_t(x, t)$ and the elastic expressions given in (18) and

$$F(t) = \frac{1}{1 + bt^q} \frac{\sin \pi n(t)}{\pi n(t)}$$

$$n(t) = qbt^q/(1 + bt^q)$$

with $b = 0.046$ and $q = 0.19$.

It is interesting to note that for the particular geometric and physical values for the adhesive-layer employed in the present problem the quasi-elastic approach yielded results which were almost indistinguishable from the collocated inversion. This fortuitous circumstance could not be anticipated *a priori* because the transformed expressions, (24) and (25), do exhibit large curvatures in the η domain. In general, the usefulness of a quasi-elastic method must be verified in such circumstances. In the present case expressions (27) are certainly easier to evaluate than (25).

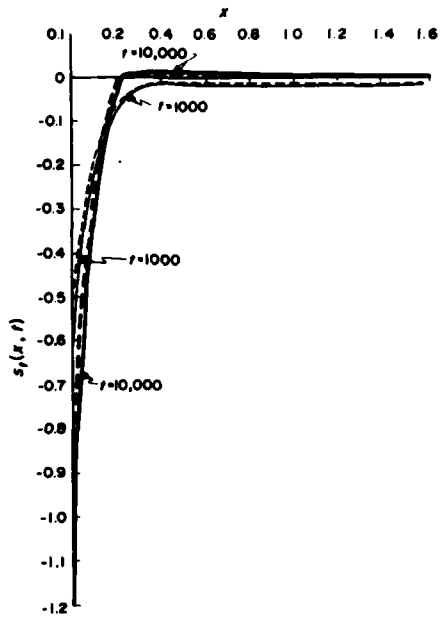

Fig. 9. Elastic and viscoelastic values of the non-dimensional tangential interlaminar traction s_t at times $t = 1000$ sec and $t = 10{,}000$ sec vs x. Dashed lines—elastic, solid lines—viscoelastic.

Employing (27), values of $s_n^{v.e}(x, t)$ and $s_t^{v.e}(x, t)$ were calculated for fixed values of time, $t = 1000$ sec and 10,000 sec, along the interface between the adhesive and adherend. These results are shown in Figs. 8 and 9 for $0 \le x \le 1.6$. (For comparison purposes, the elastic values are also shown in dashed lines.)

5. VISCOELASTIC SOLUTION UNDER FLUCTUATING AMBIENT HUMIDITY

Thus far the adhesive-layer was considered to be subjected to a sudden exposure to ambient humidity at time $t = 0$, with a swelling conversion factor A.

For fluctuating ambient humidity $A = A(t)$ the interlaminar stresses are given by a superposition integral as follows

$$s_m^{v.e}(x, t) = \int_0^t s_m^{v.e}(x, t - t') \frac{d\,A(t')}{dt'} dt' \tag{28}$$

where $m = n$ or t.

In (28) the kernel functions, under the integral sign, are given by (27).

A sample computation was performed for a sudden exposure to 100% R.H. followed by drying at time $t = t_1$ later. In this case

$$A(t) = A[H(t) - H(t - t_1)] \tag{29}$$

whereby

$$s_m^{v.e}(x, t) = s_m^{v.e}(x, t) - s_m^{v.e}(x, t - t_1) \qquad (m = n \text{ or } t). \tag{30}$$

Results for $t_1 = 10{,}000$ sec. at $x = 0.01$, $x = 1.0$ and $x = 3.0$ are shown by the dashed lines in Figs. 2–7. Note that the superposition of wetting and subsequent drying is algebraically additive in the elastic case. Therefore, all the elastic stresses, represented by thin dashed lines in Figs. 2–7, tend to zero as $t \to \infty$ *without any further sign changes.*† However, in the viscoelastic case,

†There is nevertheless an exception in Fig. 3.

the drying effects are superimposed on a *relaxed* wet state and this causes an overcompensation—thereby introducing sign-reversals in the stresses. Eventually, as $t \to \infty$, the viscoelastic stresses too tend to zero.

It is observed that viscoelasticity predicts detrimental effects that are caused by fluctuations in relative humidity—such as low cycle fatigue and interfacial tension—that are absent in an elastic analysis.

6. CONCLUDING REMARKS

The present analysis is based on several idealizations which restrict the validity of the results. The exceedingly large stresses which are predicted by linear theories near the corners $X = 0$, $Y = \pm a$ cannot be borne by real adhesives and the response in those regions must be represented by a suitable non-linear model.

In addition, the actual viscoelastic response of resins depends on the moisture content, which introduces yet another non-linearity into the analysis of adhesive layers.

The evaluation of those non-linear effects still awaits an appropriate characterization at the present time. Once available it would require solution by means of numerical methods.

Acknowledgements—The author wishes to thank Professor R. A. Schapery for many valuable discussions and Dr. S. B. Raju for his assistance in obtaining the numerical results presented herein. The author is greatly indebted to Messrs. J. E. Halkias and E. L. McKague of General Dynamics Corporation, Fort Worth, Texas for much of the information concerning the response of resins to moisture.

This work was conducted under Contract F-49620-78C-0034 from the Air Force Office of Scientific Research (AFOSR).

REFERENCES

1. Y. Weitsman, Stresses in adhesive joints due to moisture and temperature. *J. Comp. Matls* **11**, 378–394 (1977).
2. C. D. Shirrell, Diffusion of water vapor in graphite/epoxy composites. A privately communicated Air Force Materials Laboratory manuscript.
3. C-H. Shen and G. S. Springer, Moisture absorption and desorption of composite materials. *J. Comp. Matls* **10**, 2–20 (1976).
4. E. L. McKague, Jr., J. E. Halkias and I. D. Reynolds, Moisture in composites: The effect of supersonic service on diffusion. *J. Comp. Matls* **9**, 1–9 (1975).
5. I. S. Gradshteyn and I. W. Ryzhik, *Table of Integrals, Series and Products*, p. 307. Academic Press, New York (1965).
6. A. Erdelyi, W. Magnus, F. Oberhettinger and F. G. Tricomi, *Tables of Integral Transforms*, Vol. I. McGraw-Hill, New York (1954).
7. *Handbook of Mathematical Functions* (Edited by M. Abramowitz and I. A. Stegun). National Bureau of Standards (1964).
8. S. W. Beckwith, Viscoelastic characterization of a nonlinear glass/epoxy composite, including the effect of damage. Ph. D. Dissertation, Texas A&M University, (1974).
9. R. D. Maximov, Ye. A. Sokolov and V. P. Mochalov, Effect of temperature and humidity on creep of Polymeric materials. *Mechanica Polimerov* 3, 393–399 (1975) (In Russian).
10. F. W. Crossman, R. E. Mauri and W. J. Warren, Moisture Altered Viscoelastic Response of Graphite-Epoxy Composites. Lockheed Palo Alto Research Laboratory Report. *Symp. Environmental Effects on Advanced Comp. Matls.*, sponsorred by ASTM D30 Committee, Dayton, Ohio (1977).
11. Y. C. Fung, *Foundations of Solid Mechanics*, p. 417. Prentice-Hall, New Jersey (1965).
12. Y. C. Fung, *Foundations of Solid Mechanics*, p. 414. Prentice-Hall, New Jersey (1965).
13. R. A. Schapery, Stress analysis of viscoelastic materials. *J. Comp. Matls* **1**, 228–266 (1967); especially pp. 246–247.
14. J. D. Ferry, *Viscoelastic Properties of Polymers*, p. 77. Wiley, New York (1961).

Reprinted from JOURNAL OF APPLIED MECHANICS, *Vol. 46, No. 3, September 1979*

Y. Weitsman

Professor,
Civil Engineering Department,
Texas A & M University,
College Station, Texas 77843
Mem. ASME

Residual Thermal Stresses Due to Cool-Down of Epoxy-Resin Composites

This paper concerns the residual thermal stresses that develop within the resin of a fiber-reinforced composite-laminate as the material is cooled from cure temperature down to room temperature. The calculations presented herein consider the viscoelastic response of the resin and account for the temperature dependence and the stress sensivitity of the creep compliance. Comparisons with linear elasticity indicate that viscoelastic relaxation may reduce the residual stresses by about 20 percent.

Introduction

Linear elastic stress analysis predicts that the thermal stresses, which develop within a composite material due to typical temperature excursions experienced by the structure, may exhaust the strength of various laminae even before the application of external loads. Effects which were attributed to high residual thermal stresses in composite laminates were reported by several investigators [1, 2]. A similar prediction can be made for the micromechanical thermal stresses within the epoxy resin when its response is assumed to follow linear thermoelasticity. The assumption of linear-elastic behavior tends to overestimate the residual thermal stresses and, by ignoring the time, temperature, and stress dependencies of the resin's response rules out any advantage that may accrue from the consideration of special temperature histories.

A major portion of the thermal stress is introduced into the composite laminate during cooling from cure temperature down to room temperature. This cool-down stage may be viewed as part of the manufacturing process and therefore lends itself to careful control. It has already been shown that the selection of an optimal cool-down path could reduce residual thermal stresses in plexiglass [3] and the same idea can be carried over to epoxy and epoxy-based composites.

This paper presents calculations of the "micromechanical" residual stresses within the epoxy due to cool-down. Our purpose is to provide a quantitative assessment of the role of inelastic response. The calculations are based upon a thermorheologically complex viscoelastic model, which includes some aspects of the nonlinearity that is attributed to stress effects on relaxation.

The findings of this paper are preliminary since they are based upon incomplete data. Consequently it was necessary to extrapolate existing data to higher temperature ranges and to infer the nonlinear stress-effects by analogy from similar materials (glass-reinforeced epoxy). Perhaps most significantly, due to the complete lack of data, it was necessary to omit any aging effects, which may be very prominent during the cool-down of a newly created laminate.

Several experimental programs, currently in progress, should provide information which would enable us to reassess and refine the model which is used in the present work.

Formulation

Consider a fiber-reinforced, multidirectional, composite laminate $-h \le z \le h$, $-\infty < x,y < \infty$, traction-free at the boundaries $z = \pm h$ and subjected to spatially uniform temperature fluctuations. For sufficiently slow fluctuation of the ambient temperature and sufficiently thin layers it is possible to discard the transient states and consider the quasi-static case of uniform temperature $\theta(z,t) \cong \theta(\pm h,t) = \theta(t)$.[1]

Since the present analysis aims at investigating the thermo-viscoelastic response of the resin let us assume that the multidirectional fibers, all of which lie in planes z = const., affect the behavior of the resin through the following geometric constraint

$$\epsilon_x = \epsilon_y = \alpha_f \Delta\theta \tag{1}$$

In (1) α_f is the coefficient of thermal expansion of the fibers, $\Delta\theta$ is

Contributed by the Applied Mechanics Division for presentation at the Winter Annual Meeting, New York, N.Y., December 2-7, 1979, of THE AMERICAN SOCIETY OF MECHANICAL ENGINEERS.

Discussion on this paper should be addressed to the Editorial Department, ASME, United Engineering Center, 345 East 47th Street, New York, N. Y. 10017, and will be accepted until December 1, 1979. Readers who need more time to prepare a Discussion should request an extension of the deadline from the Editorial Department. Manuscript received by ASME Applied Mechanics Division, June, 1978; final revision, December, 1978. Paper No. 79-WA/APM-9.

[1] In typical laminates, the transient effects may be ignored up to temperature fluctuations of 5°K/min.

the difference between the initial and final temperatures, $\Delta\theta = \theta_0 - \theta_f$, and ϵ_x, ϵ_y are the in-plane strains.

If we assume in-plane isotropy of the layer, and consider linear-elastic response, we obtain the following results [3]:

$$\sigma_x = \sigma_y = \sigma = -cG\Delta\theta$$
$$\sigma_z = 0 \quad \text{and all shears vanish.} \tag{2}$$

where

$$c = 2\frac{1+\nu}{1-\nu}(\alpha_m - \alpha_f). \tag{2'}$$

In (2) and (2') G, ν are the shear modulus and Poisson's ratio of the resin, and α_m is its coefficient of thermal expansion.

If the resin responds viscoelastically equation (2) takes the form

$$\sigma(t_f) = -c\int_0^{t_f} G[\xi(t_f) - \xi(t')]\dot{\theta}(t')dt' \tag{3}$$

where ξ is a "reduced time," given by

$$\xi(u) = \int_0^u \frac{ds}{\alpha_T(s)} \tag{4}$$

and $G(t)$ is the shear-relaxation function for the resin.

The purpose of the subsequent investigation is to consider and evaluate the significance of various factors which affect the function α_T, and investigate the influence of the history $\theta(t)$ on $\sigma(t_f)$.

A Linear Thermorheologically Complex Model for Epoxy

On the basis of uniaxial tension data obtained for "shell 58-68R" epoxy resin [4], for temperatures ranging between 20°F and 160°F, it is possible to express the creep compliance as follows:

$$D(\theta,t) = D_0(\theta) + D_1\left[\frac{t}{\alpha_T(\theta)}\right]^q \tag{5}$$

where

$$D_0(\theta) = [0.2731 + 0.000574\,(\theta - 297)]\,10^{-6}$$

$$D_1 = 0.01 \times 10^{-6}, \quad \alpha_T(\theta) = \exp\left(\frac{6480}{\theta} - 21.82\right), \quad q = 0.19$$

In (5), D is in $(\text{kPa})^{-1}$, the time t is in minutes, and the temperature θ is in degrees Kelvin. Furthermore, the Poisson ratio for epoxy is approximately constant $\nu = 0.35$. For temperatures below glass transition the coefficients of thermal expansion yield that

$$\alpha = \alpha_m - \alpha_f = 5 \times 10^{-5}\text{m/m/1°K}.$$

Consider a composite cooled-down between a cure-temperature $\theta_0 = 438$°K and room temperature $\theta_f = 298$°K. For lack of more complete data assume that (5) can be extrapolated up to the elevated cure-temperature. In terms of the imposed thermal strain $(\alpha_m - \alpha_f)(\theta_0 - \theta(t))$ and the creep compliance (5) we obtain the following integral equation for the stress σ:

$$\frac{\alpha}{1-\nu}[\theta_0 - \theta(t)] = D_0(\theta)\sigma(t) + D_1\int_0^t [\xi(t) - \xi(t')]^q\dot{\sigma}(t')dt' \tag{6}$$

where $\alpha = \alpha_m - \alpha_f$.

If the temperature drops linearly between θ_0 and θ_f over a time interval t_f then

$$\theta(t) = \theta_0 + Rt \quad \text{with} \quad R = (\theta_f - \theta_0)/t_f$$

and equation (6) reads

$$-\frac{\alpha}{1-\nu}Rt = D_0(\theta_0 + Rt)\sigma(t) + D_1\int_0^t\left[\int_0^t \frac{ds}{\alpha_T(\theta(s))} - \int_0^{t'}\frac{ds}{\alpha_T(\theta(s))}\right]^q\dot{\sigma}(t')dt' \tag{7}$$

where in (7)

$$\alpha_T(\theta(s)) = \exp\left(\frac{6480}{\theta_0 + Rs} - 21.82\right)$$

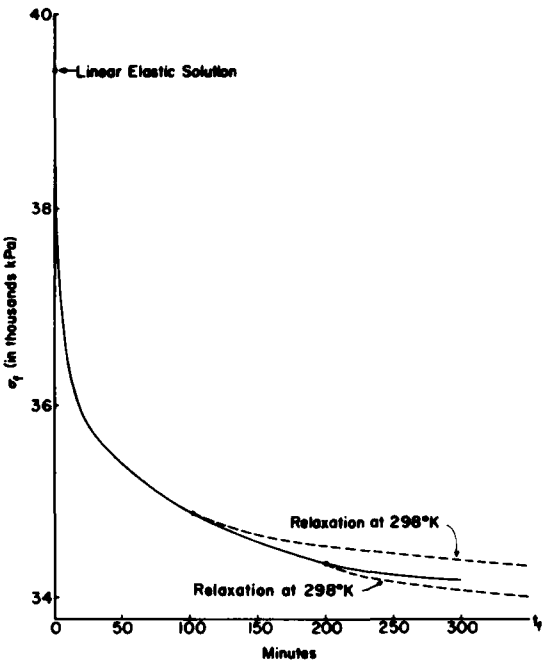

Fig. 1 Dependence of the residual stress σ on cooling time t_f; linear thermorheologically complex model. Linear (constant-rate) cool-down from θ_0 = 438°K to θ_f = 298°K. Dashed lines indicate further relaxation of residual stresses at θ_f = 298°K after termination of cool-down.

The solution of (7) was obtained numerically. Following the scheme developed in reference [3], the time interval t_f was divided into subintervals $\Delta t = t_f/\eta$ and each intermediate time was denoted by $t_j = j\Delta t$. Denoting $\theta_j = \theta(t_j) = \theta_0 + Rt_j$, $\sigma_j = \sigma(t_j)$ and computing the n-values of

$$\xi_j = \xi(t_j) = \int_0^{t_j}\frac{ds}{\alpha_T(\theta(s))}$$

and n-values of $D_{0j} = D_0(\theta_j) = [0.2371 - 0.000574(\theta_j - 297)]\,10^{-6}$ the following expression was obtained for σ_j

$$\sigma_j = \frac{1}{D_{0j} + 1/2(\xi_j - \xi_{j-1})^q}\left\{-\frac{\alpha}{1-\nu}Rt_j + \frac{1}{2}D_1(\xi_j - \xi_{j-1})^q\sigma_{j-1} - \frac{1}{2}D_1H(j-2)\sum_{m=1}^{j-1}[(\xi_j - \xi_m)^q + (\xi_j - \xi_{m-1})^q](\sigma_m - \sigma_{m-1})\right\} \tag{8}$$

In (8), $H(j-2)$ is a unit step function which vanishes for $j < 2$. In addition, it is necessary to employ the initial conditions $\sigma_0 = 0$, $\xi_0 = 0$.

Calculations were performed on an Amdahl 470 computer. The residual stress at the termination of cool-down is shown in Fig. 1 as a function of the time t_f allowed for the cooling. The reduction in the residual stress with the increase in cooling-time t_f is due to viscoelastic relaxation. The value of $\sigma = 39430$ kPa at $t_f = 0$ corresponds to the linearly elastic case.

Additionally relaxation of stresses occurs, at $\theta = \theta_f$, at times $t > t_f$. The calculation of these stresses requires a slight modification of expressions (7) and (8), which is omitted here. The additonal relaxation, which is drawn by the dashed lines in Fig. 1, further reduces the residual stresses by about 3–4 percent.

Optimal Cool-Down Path for the Thermorheologically Simple Model

It has been shown previously [3] that, for a prescribed time t_f for cool-down, there exists an optimal cool-down path $\theta = \theta(t)$ which minimizes the residual stress σ_f. A remarkable feature of this optimal path is that it contains discontinuities at times $t = 0$ and $t = t_f$. It is

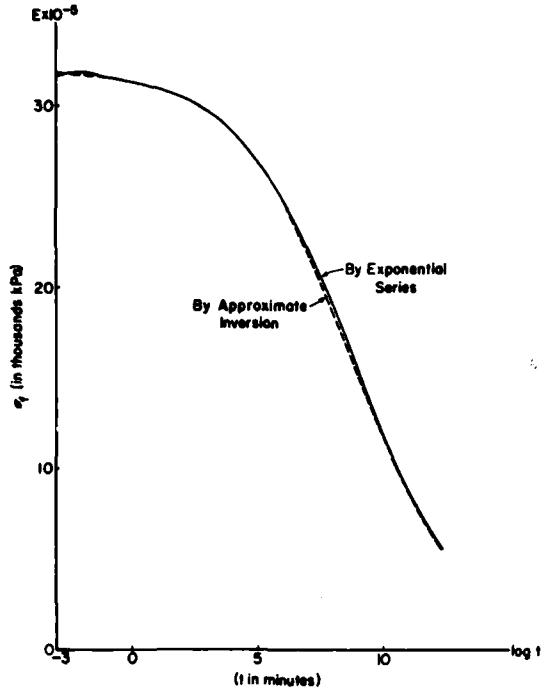

Fig. 2 Relaxation modulus $E(t)$ obtained by approximate inversion of $D(t)$ as given in equation (11) (dashed line) and by exponential-series determined through collocation (solid line)

interesting to note that the discontinuous character of the solution is apparently quite common, since a similar result was obtained recently for optimal strain paths [5].

In order to reduce the computational effort consider the approximate form of the creep compliance

$$D(t) = b(1 + at^q)$$

where

$$b = 0.3126 \times 10^{-6}\ (\text{kPa})^{-1}, \quad a = 0.032, \quad q = 0.19 \tag{9}$$

Equation (9) was derived from (5), with $\theta = 75°\text{F}$ (297°K) and when $D_0(\theta)$ is approximated by a constant value $D_0 = b$.

Furthermore, it is more convenient to employ the relaxation modulus $E(t)$ instead of the compliance $D(t)$. This task is accomplished with the aid of Laplace transforms. The Laplace transform of $D(t)$ yields

$$p\bar{D}(p) = b\left[1 + a\frac{\Gamma(q+1)}{p^q}\right] = \frac{1}{p\bar{E}(p)} \tag{10}$$

where $\bar{E}(p)$ is the Laplace transform of $E(t)$ [6]. An approximate inversion, based upon the expression [7]

$$E(t) \simeq \frac{1}{p\bar{D}(p)}\bigg|_{p=1/2t}$$

yields

$$E(t) = \frac{3.2 \times 10^6}{1 + 0.0336t^{0.19}}\ \text{kPa} \tag{11}$$

The validity of (11) was verified by comparison with a collocation scheme for the inversion of (10). The collocation method will be discussed in the following section on nonlinear effects. The comparison is shown in Fig. 2.

Employment of (11) in (3) yields

$$\sigma(t_f) = -c_1 S(t_f) \tag{12}$$

where

$$S(t_f) = \int_0^{t_f}\left\{1 + a\left[\int_{t'}^{t_f}\frac{ds}{\alpha_T(s)}\right]^q\right\}^{-1}\dot{\theta}(t')dt' \tag{13}$$

and

$$c_1 = \frac{3.2 \times 10^6 \alpha}{1 - \nu}$$

Also, in (13)

$$\alpha_T = \exp\left[\frac{6480}{\theta(s)} - 21.82\right]$$

To determine the optimal path $\theta(t)$ subdivide t_f into n equal portions as before and consider a "stair-case" drop in θ

$$\theta(t) = A_k, \quad t_k < t < t_{k+1}, \quad 0 \le k \le n-1$$

whereby

$$\dot{\theta}(t) = (A_k - A_{k-1})\,\delta(t - t_k), \quad 1 \le k \le n \tag{14}$$

and

$$\dot{\theta}(t) = (A_0 - \theta_0)\,\delta(t), \quad k = 0$$

Substitution of (14) into (13) gives

$$S(t_f) = \frac{A_0 - \theta_0}{1 + a\left\{\Delta t\sum_{j=0}^{n-1} 1/\alpha_T(A_j)\right\}^q} + \sum_{k=1}^{n-1}\frac{A_k - A_{k-1}}{1 + a\left\{\Delta t\sum_{j=k}^{n-1} 1/\alpha_T(A_j)\right\}^q} - (A_{n-1} - \theta_f) \tag{15}$$

Equations (12) and (15) express the residual stress $\sigma(t_f)$ in terms of the unknown intermediate temperatures, $A_j = A(t_j)\ j = 0, 1, \ldots n-1$.

For a stationary value it is necessary that $\partial S(t_f)/\partial A_j = 0, j = 0, 1 \ldots n-1$. This results in n simultaneous equations in the n unknown A_j as follows:

$$\frac{A_0 - \theta_0}{Z_0^2}\frac{\partial Z_0}{\partial A_k} + H(i-1)\sum_{i=1}^{k}\frac{A_i - A_{i-1}}{Z_i^2}\frac{\partial Z_i}{\partial A_k} + \frac{1}{Z_{k+1}} - \frac{1}{Z_k} = 0$$
$$k = 0, 1, \ldots n-1 \tag{16}$$

where, in (16) $Z_n = 1$, $H(i-1)$ is the unit step-function which vanishes for negative arguments, and

$$Z_j = 1 + a\left\{\Delta t\sum_{j-i}^{n-1} 1/\alpha_T(A_j)\right\}^q$$

$$\frac{\partial Z_j}{\partial A_k} = -6480\,A_k^{-2}\left\{\Delta t\sum_{j=i}^{n-1} 1/\alpha_T(A_j)\right\}^q$$

The solution of (15) and (16) was obtained by an iteration technique.[2] The resulting optimal path is shown in Fig. 3 for $t_f = 100$ min. It is worth noting that the value of $\sigma(t_f)$ is insensitive to the details of the "tail-end" of the path, i.e., near t_f. Cooling along the optimal path results in a residual stress $\sigma(t_f) = 32900$ kPa. This represents an improvement of about 6 percent over the linear cool-down path.

Stress Effects on Relaxation During Cool-Down

We note that the residual stresses reach levels which exceed half the ultimate stress of epoxy, $\sigma_u = 52{,}200$ kPa. Stresses of such magnitude were found to influence the creep-response of epoxy-based composites [9]. The stress effect can be incorporated into the "shift factor" α_T of equation (4) as follows:

[2] We refrained from using standard optimization methods, because those techniques presuppose a smooth functional which can be approximated by quadratic function (see, e.g., reference [8]) while the present case revolves about a discontinuous function.

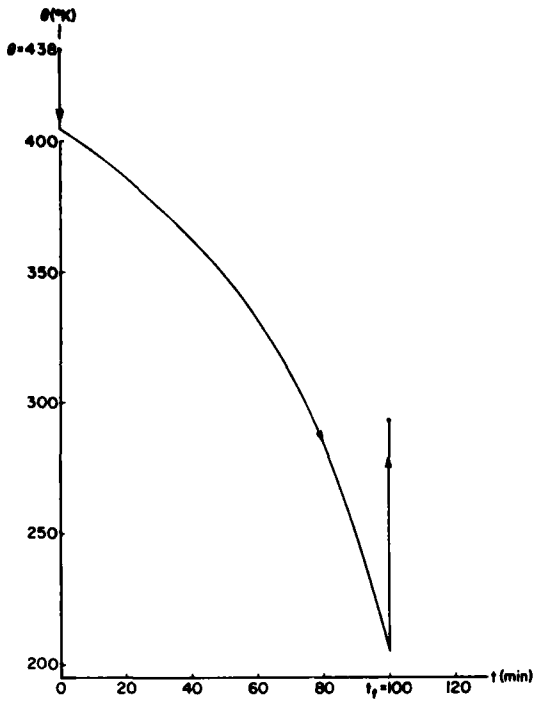

Fig. 3 Optimal cool-down path for the thermorheologically complex model

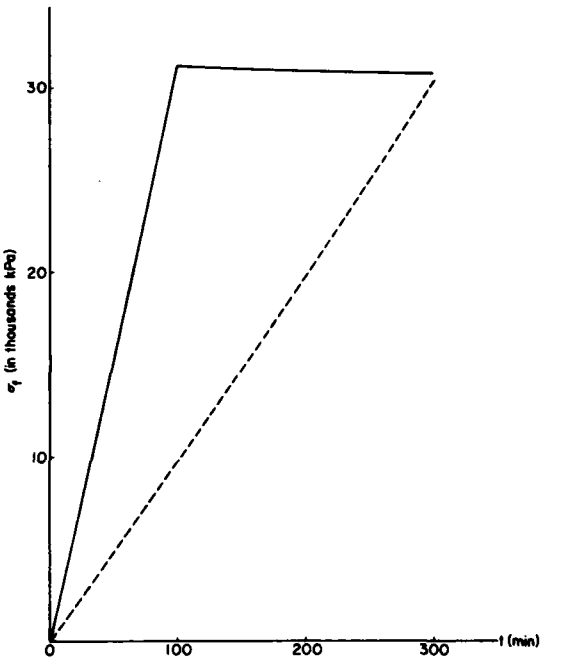

Fig. 4 Variation of residual stress σ with time t. Stress effected relaxation (equation (17)). Linear (constant-rate) cool-down from $\theta_0 = 438°K$ to $\theta_f = 293°K$. Solid line corresponds to cooling time $t_f = 100$ min and also shows relaxation beyond termination of cool-down. Dashed line corresponds to $t_f = 300$ min.

$$\alpha_T(\sigma,\theta) = \exp\left\{\frac{A/\theta_R - (B/\theta_R)H[\sigma - \sigma_c(\theta)][\sigma - \sigma_c(\theta)]/\sigma_u(\theta)}{\theta/\theta_R} - \frac{A}{\theta_R}\right\} \quad (17)$$

In (17) θ_R is a reference absolute temperature, σ_c is a "threshold stress" beyond which stress starts to affect α_T, σ_u is the ultimate stress of the resin, $H(\ )$ is a unit step-function which vanishes for negative arguments and A, B are material constants.

From the data given in reference [9], which were obtained at a reference temperature $\theta_R = 293°K$, and from recent data which detailed the dependence of σ_u on θ [10], the following values were selected:

$$A = 6500, \quad B = 2000$$

$$\sigma_u(\theta) = 55200 - 190(\theta - \theta_R)$$

$$\sigma_c(\theta) = 13800 - 47.5(\theta - \theta_R).$$

where σ_u and σ_c are in kPa.

A significant reduction in the computational effort is achieved if the relaxation function $E(t)$, as given in (11), is expanded in a sum of exponentials. To this purpose, the method of collocation [7] was employed and $E(t)$ was expressed as

$$E(t) = \sum_{I=1}^{22} E_I e^{-\lambda_I t} \quad \lambda_I = 10^{-18}, 10^{-17}, \ldots 10^{3} \quad (18)$$

The values of E_I, which are not listed here, were obtained from solving the simultaneous equations

$$\sum_{I=1}^{22} (1 + \lambda_I/\lambda_J)^{-1} E_I = p\bar{E}(p)_{|p=\lambda_J}$$

with $p\bar{E}(p)$ given in (10). The form (18) of $E(t)$ is shown in Fig. 2.

Substitution of (17) and (18) in (3) and (4) yields

$$\sigma(t) = \sum_{I=1}^{22} E_I \int_0^t \exp\left[-\lambda_I \xi(t) + \lambda_I \xi(t')\right] \frac{d\epsilon}{dt'} dt' \quad (19)$$

where

$$\xi(u) = \int_0^u \frac{ds}{\alpha_T[\theta(s),\sigma(s)]}$$

with the form of α_T given in (17).

Consider a linear cool-down from θ_0 to θ_f during a time interval t_f. Denote the constatnt cooling rate by $R = (\theta_0 - \theta_f)/t_f$ and let $c_2 = \alpha R/(1 - \nu)$. In this case (19) reduces to

$$\sigma(t) = c_2 S(t)$$

where

$$S(t) = \sum_I E_I \int_0^t \exp\left[-\lambda_I \xi(t) + \lambda_I \xi(t')\right] dt' \quad (20)$$

Divide the time interval t_f into n equal intervals Δt and denote $t_k = k\Delta t$ as before. The initial condition is $\sigma_0 = 0$ and the intermediate temperatures are $\theta_k = \theta_0 - Rt_k$. If we employ the approximation that

$$\alpha_T(\sigma,\theta) \simeq \alpha_T(\sigma_k,\theta_k) \quad \text{for} \quad t_k < t < t_{k+1} \quad (21)$$

then, as a consequence of expansion (18), it is possible to integrate $S(t)$ analytically over each subinterval $t_k < t < t_{k+1}$. This leads to a substantial reduction in computations.

Denote $V_k = \alpha_T(\sigma_k,T_k)$ and $W_k = e^{-V_k}$. From (21) it follows that

$$\xi_k = \xi(t_k) = \sum_{i=1}^{k} (t_i - t_{i-1}) W_{i-1}$$

Denote further

$$\Psi_{rk} = \sum_{m=0}^{r-1} (t_m - t_{m-1}) W_{m-1} - \xi_k \qquad (r = 1, \ldots k.\ k = 1, \ldots n)$$

and

$$\phi_{rk} = \Psi_{rk} + W_{r-1}(t_r - t_{r-1})$$

Straightforward manipulations lead to

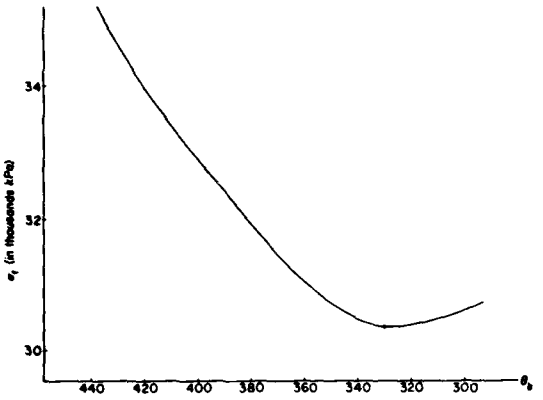

Fig. 5 Two-step cool-down; variation of the residual stress σ with the intermediate-level temperature θ_b. $\theta_0 = 438°K$, $\theta_f = 293°K$, $t_f = 100$ min. Note minimal residual stress at $\theta_b = 333°K$.

$$S_k = S(t_k) = \sum_{I=1}^{22} E_I \left\{ \sum_{r=1}^{k} (\lambda_I W_{r-1})^{-1} \times [\exp(\lambda_I \phi_{rk}) - \exp(\lambda_I \Psi_{rk})] \right\} \quad (22)$$

and

$$\sigma_k = c_2 S_k$$

For times beyond termination of cool-down $t_k > t_f$, the temperature retains a constant value θ_f but the stress σ_k continues to relax. The computational scheme (22) remains valid except that now, $\alpha_T(\sigma_k,\theta_k) = \alpha_T(\sigma_k,\theta_f)$, $(t_K > t_f)$.

Results for a constant cooling rate from $\theta_0 = 438°K$ down to $\theta_f = 293°K$ are shown in Fig. 4 for $t_f = 100$ min, followed by a relaxation at 293°K, and for $t_f = 300$ min. Note that a prolongation in the cool-down time does not effectively reduce the residual stresses. Comparison with results based upon the lineal thermorheologically complex model shows that when stress effects are incorporated into α_T, equation (17), the relaxation is enhanced and the residual stresses reduce by an additional amount of 10 percent.

Finally, consider the case of a "two-step cooling." In this case the temperature is dropped suddenly from θ_0 to θ_b, held at $\theta = \theta_b$ for a period $t = t_f$ and dropped sharply again to $\theta = \theta_f$ at $t = t_f$. For such cooling-history equation (19) yields

$$\sigma(t_f) = c_m S(t_f) + c_f \sum_I E_I \quad (23)$$

In equation (23)

$$c_m = \frac{\alpha}{1-\nu}(\theta_0 - \theta_b), \quad c_f = \frac{\alpha}{1-\nu}(\theta_b - \theta_f)$$

and

$$S_i = \sum_I E_I e^{-\lambda_I \xi_i}$$

where ξ_i is defined and evaluated as before.

Following a numerical scheme similar to (22), the dependence of the residual stress $\sigma(t_f)$ on the intermediate temperature θ_b has been computed for a "hold-time" $t_f = 100$ min. In the calculations we took $\theta_0 = 438°K$ and $\theta_f = 293°K$. The results are shown in Fig. 5.

Note that the residual stress attains a minimum at the intermediate temperature $\theta_b = 333°K$. A similar behavior was observed experimentally for epoxy coupons reinforced by unidirectional fibers. Those coupons were cooled-down in two-steps and a qualitative assessment of the residual stresses was obtained by means of a frozen fringe pattern. It was observed that a minimal fringe count was attained at an intermediate value of temperature $\theta_b (\theta_f > \theta_b > \theta_0)$.[3]

Concluding Remarks

It has been shown that a linear elastic analysis of residual stresses overestimates their magnitude by more than 20 percent. If account is taken of the viscoelastic response of the material it may be possible to design a cool-down path that will yield a reduced value of residual stresses. It seems that the details of the cool-down path influence the magnitude of the residual stresses more noticeably than the duration of the cooling period.

The computations conducted in the present paper are based upon incomplete data. It is intended to modify the calculations and analysis in light of new data as they become available. It should be noted that the effects of aging were not considered in the present formulation. These effects may be of prime importance because it is conceivable that the newly created epoxy may be undergoing rapid aging while it is being cooled down. An inquiry into this matter is now under way.

Acknowledgments

The author wishes to thank Prof. R. A. Schapery for many helpful discussions and Prof. J. Ham for several useful comments. The assistance of Dr. S. B. Raju in obtaining the numerical results presented herein is gratefully acknowledged. This work was conducted under Contract F49620-78C-0034 from the Air Force Office for Scientific Research (AFOSR).

References

1 Chamis, C. C., "Residual Stresses in Angleplied Laminates and Their Effects on Laminate Behavior," NASA Report NASA TM-78835, Apr. 1978.

2 Hahn, H. T., and Pagano, N. J., "Curing Stresses in Composite Laminates," *Journal of Composite Materials*, Vol. 9, 1975, pp. 91–106.

3 Weitsman, Y., and Ford, D., "On the Optimization of Cool-Down Temperatures in Viscoelastic Resins," *Recent Advances in Engineering Science, Proceedings, 14th Annual Meeting of the Society of Engineering Science*, Sih, G. C., ed., 1977, pp. 323–339.

4 Beckwith, S. W., "Viscoelastic Characterization of a Nonlinear Glass/Epoxy Composite Including the Effect of Damage," PhD dissertation, Texas A&M University, Dec. 1974.

5 Gurtin, M. E., McCamy, R. C., and Murphy, L. F., "On Optimal Strain Paths in Linear Viscoelasticity," forthcoming.

6 Fung, Y. C., *Foundations of Solid Mechanics*, Prentice Hall, 1965, p. 417.

7 Schapery, R. A., "Stress Analysis of Viscoelastic Composite Materials," *Journal of Composite Materials*, Vol. 1, 1967, pp. 228–266.

8 Fox, R. L., *Optimization Methods for Engineering Design*, Addison-Wesley, Chapter 2, 1973.

9 Lou, Y. C., and Schapery, R. A., "Viscoelastic Characterization of a Nonlinear Fiber-Reinforced Plastic," *Journal of Composite Materials*, Vol. 5, 1971, pp. 208–234.

10 Kibler, K., Private Communication, General Dynamics Corp., Fort Worth, Texas.

[3] The author is indebted to Dr. Frank Crossman, of Lockheed Missiles and Space Co., Palo Alto, Calif., for this information.

Residual Stresses due to Environmental Conditioning of Cross-Ply Graphite/Epoxy Laminates [§]

by

D.A. Douglass* and Y. Weitsman**

Extended Abstract

Increasing concern with the effects of temperature and moisture on the performance of composites demands the development of accelerated environmental conditioning techniques. These conditioning schemes attempt to simulate extreme exposures to moisture and temperature which may be incurred during service conditions of the composite material.

Since the diffusion of moisture proceeds at extremely slow rates, and may require months or years until saturation is reached at room temperature, the conditioning process is often accelerated by the employment of elevated conditioning temperatures which speed up the rate of moisture sorption and shorten the time of the experimental task.

It was observed that certain conditioning schemes may result in microcracking and damage to the composite laminates. In order to develop a time-saving, yet non-damaging, environmental conditioning method, a need exists for evaluating the internal stresses which arise due to moisture and temperature and assess the relative merits of various conditioning schemes.

In this paper, the moisture and temperature effects are formulated by means of a viscoelastic response. Elastic solutions are provided for purpose of comparison. The computations incorporate realistic material parameters that are based on recent data and results are presented for symmetric laminates containing 0° and 90° plies. The initial stresses

---

*Design Engineer, Bell Helicopter Textron, Fort Worth, Texas.
**Professor, Civil Engineering Department, Texas A&M University, College Station, Texas.

§To appear in the Proceedings of the 3rd International Conference on Composite Materials, August 1980.

due to cool-down from cure and due to moisture sorption during storage prior to conditioning are calculated by means of elastic analysis.

Since heat diffuses extremely rapidly and equilibrates throughout the laminate during times that are much shorter than all other characteristic times, we discard the process of heat conduction and consider spatially uniform temperature profiles for the entire conditioning stage. On the other hand, we account for the predominant effect of temperature on mositure diffusivity in solving for the moisture diffusion which, due to its extremely slow progress, is described by a time-transient and spatially non-uniform process throughout the conditioning stage.

Moisture and temperature effect the response of composites in two counter-acting ways. On one hand, both factors induce swelling strains into the material, particularly into the matrix component of the composite. Since the natural tendency to swell is resisted by geometric constraints which are always present in structures—and especially in cross-ply laminates—both moisture and temperature can be viewed as direct causes for internal stresses and are recognized as such in both the elastic and viscoelastic analyses.

On the ohter hand, both moisture and temperature strongly affect some of the material moduli of fiber-reinforced composites. These effects are most pronounced in the softening and accelerated rates of creep (or relaxation) that occur with rising temperatures and moisture levels. These last-mentioned effects tend to counteract the aforementioned influences, so that with increase in temperature and moisture an actual competition takes place between stressing on one hand and stress relief on the other. While this "competition" is accounted for in the viscoelastic analysis, it cannot be considered within the context of the elastic response.

All the above mentioned factors are included and featured in our viscoelastic analysis. In all our computations, we disregard edge effects and consider only those stress and strain fields which are several ply-thickness distance away from the edges. The elastic and viscoelastic solutions are evaluated up to the times at which the

laminates reach moisture saturation, whereupon they are cooled back to room temperature.

Some representative results are shown in Figures 1 and 2. Both figures show the stress σ_y which arises in an 8-ply laminate, which consists of two outer 0° plies and two inner 90° plies arranged symmetrically about the middle plane. The y axis coincides with the longitudinal (parallel to fibers) direction of the 90° plies and corresponds to the transverse direction in the outer, 0° plies. The stress profiles are plotted vs. the depth coordinate z across the thickness of the laminate (z = 0 at the middle plane) at times t = 1, 100, 1000 and 10,000 minutes into the conditioning stage and also at saturation, just prior and just past cooling back to room temperature.

Figure 1 provides a comparison between two conditioning schemes. Exposure to 98% R.H. at 180° F (solid line), for which saturation is reached after 22 days, and exposure to 98% R.H. at 150° F (dashed line), for which saturation is attained after 45 days. Note the substantial differences in the stress profiles for the two conditioning schemes. In particular, upon return to room temperature the stresses described by the solid lines are of opposite sign, and somewhat larger, than those given by dashed lines. In all other lay-ups, for which computations were performed, it was similarly found that conditioning at 150° F resulted in lower values for the final stresses.

Figure 2 provides a comparison between viscoelastic values (shown in solid lines) and elastic results (dashed lines). The computations were performed for conditioning at 98% R.H. and 180° F. Note the vast discrepancy between the two sets of results, especially with increasing time, indicating that by discarding stress relaxation the elastic analysis yields results that are substantially off the mark.

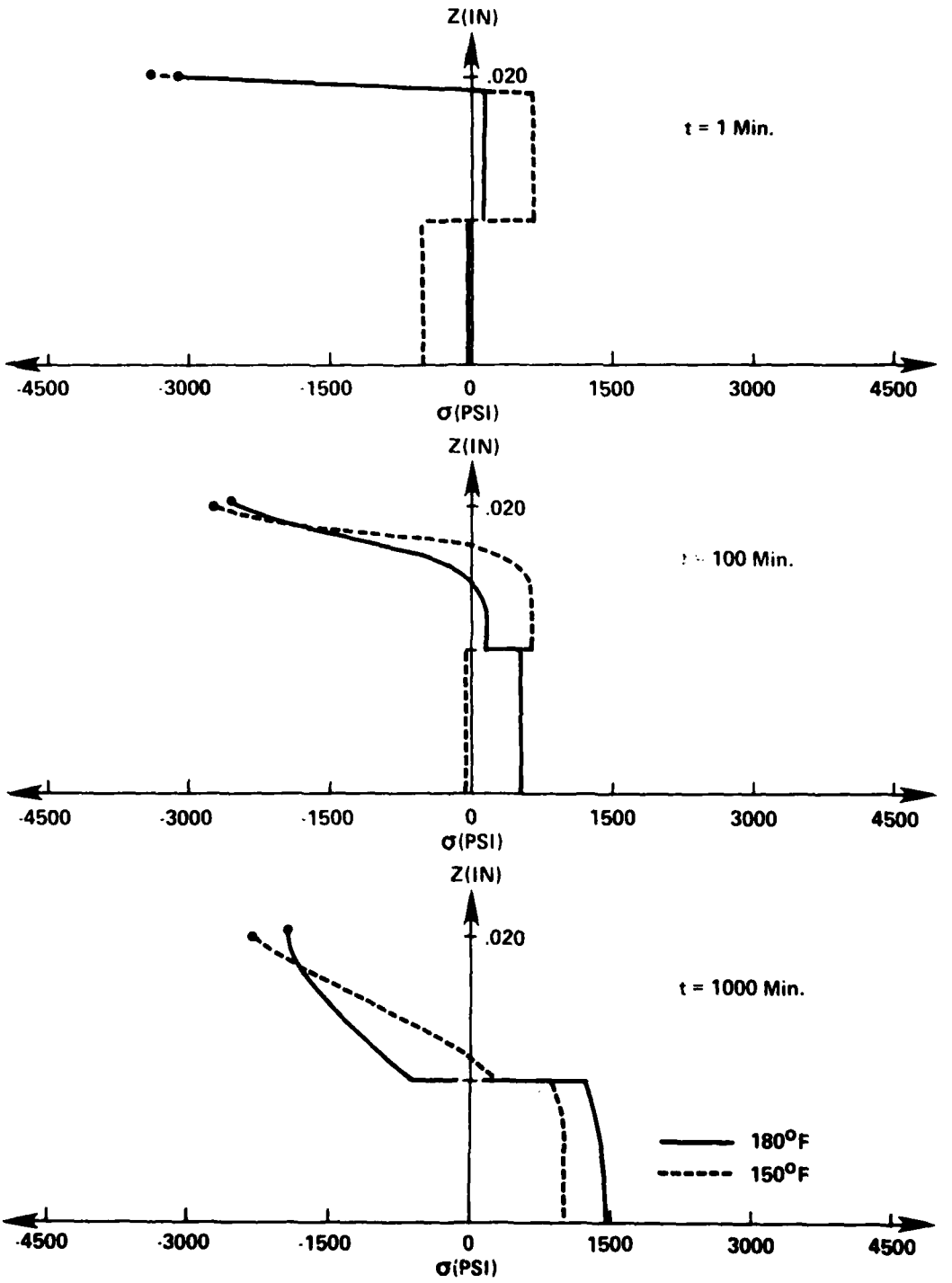

Figure 1. $[0/90]_s$ σ_y viscoelastic stresses.

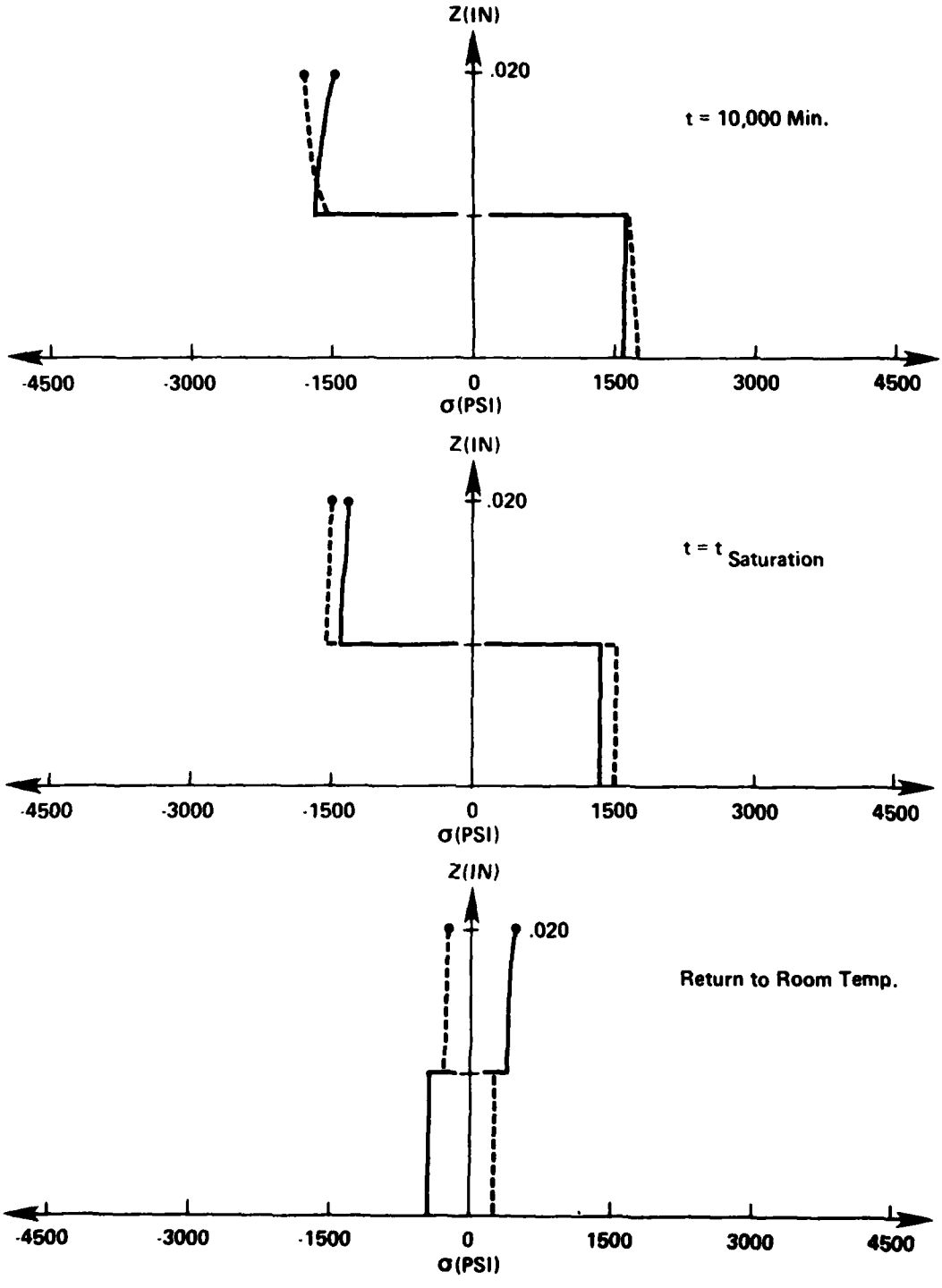

Figure 1. (continued)

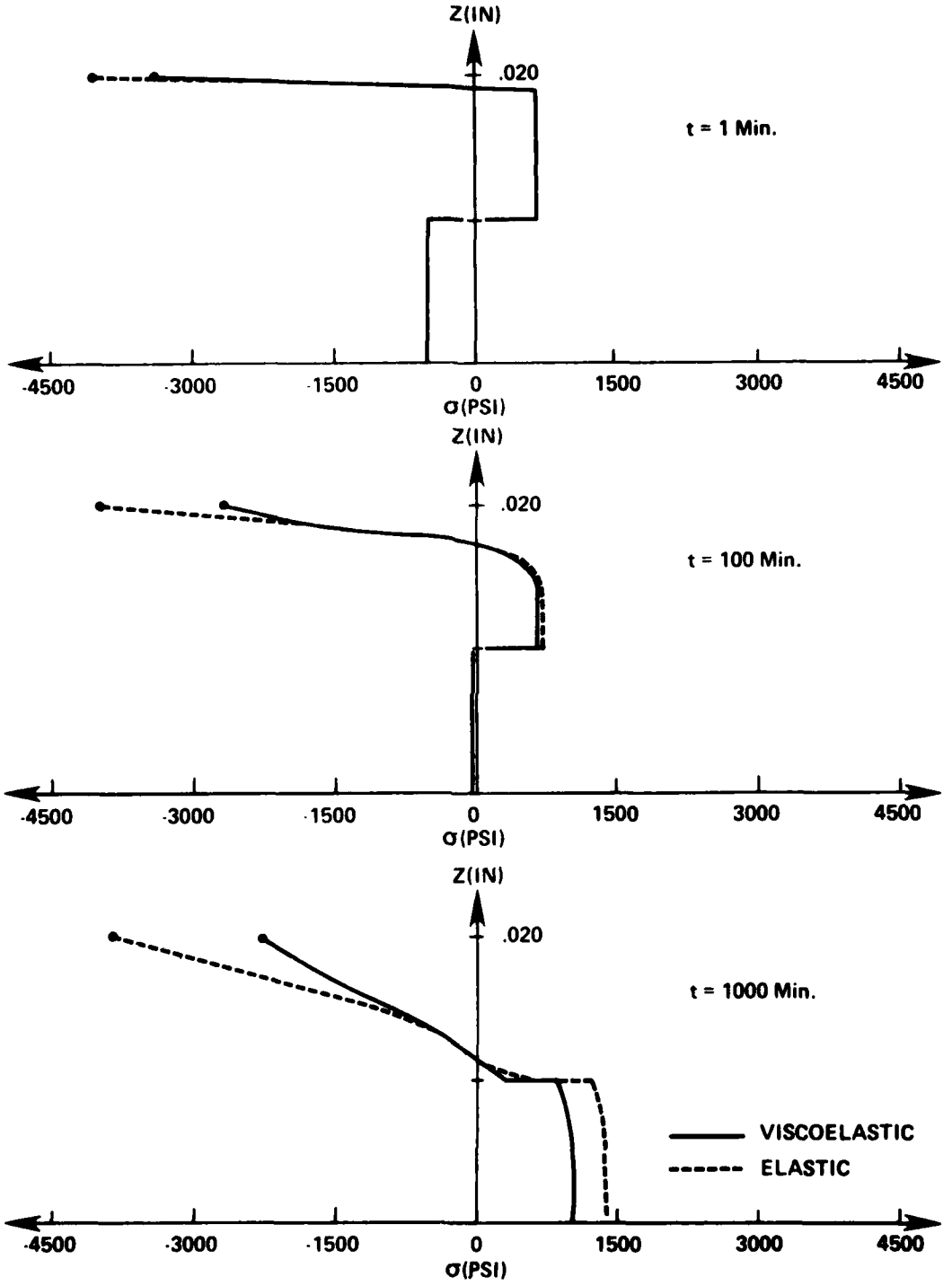

Figure 2. $[0/90]_s$ 150°F, σ_y stresses.

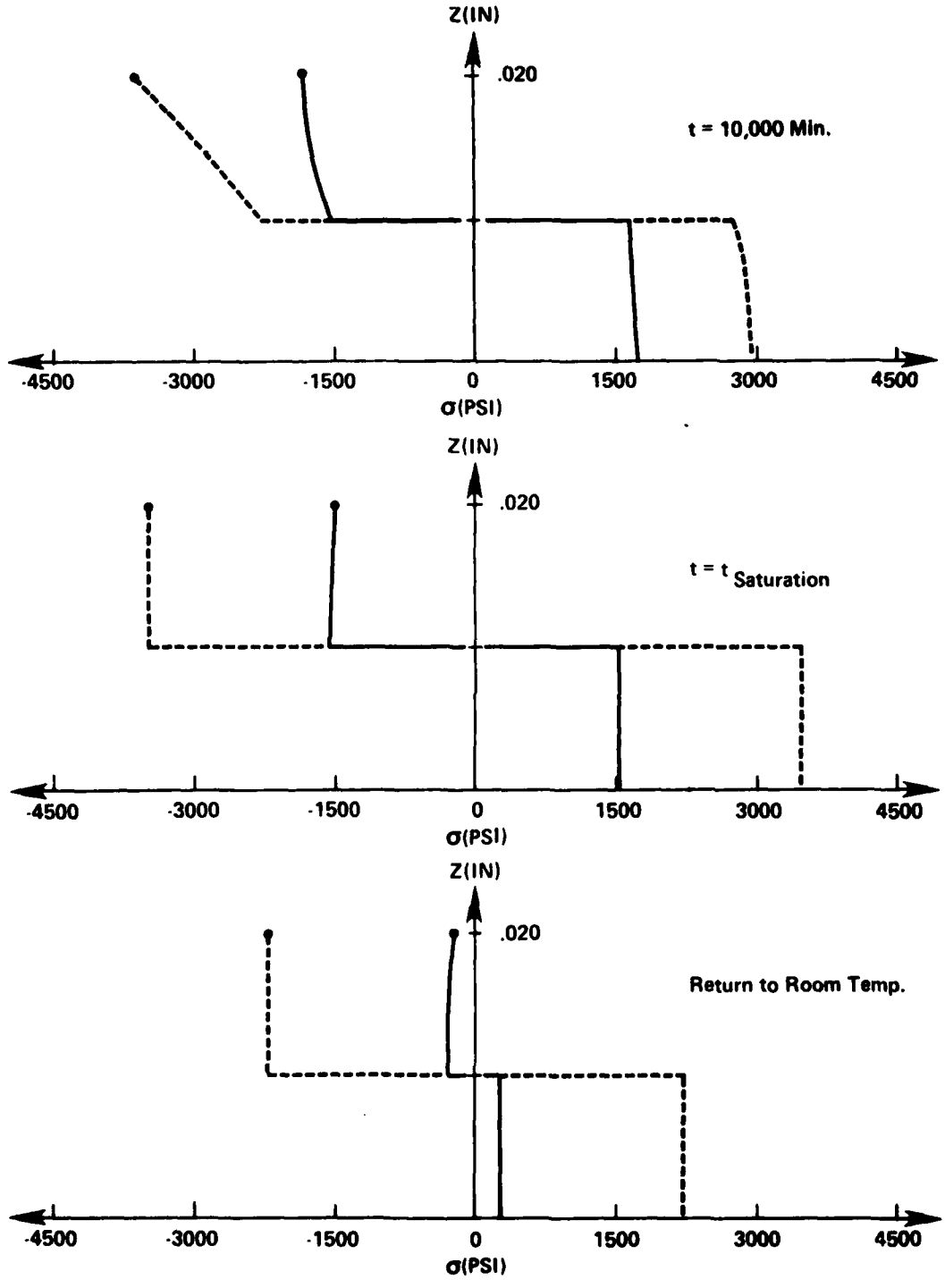

Figure 2. (continued)

Thermal Buckling of Free Plates due to Non-Uniform Temperature Distribution

by

Y. Weitsman*

This investigation concerns the buckling of thin isotropic plates due to uneven temperature distribution over their surface.

The problem is motivated by the processing and operational conditions of fiber reinforced composite laminates. It was noticed that during the cool-down of large composite structures temperature variations of up to 40°F could occur in several spotty locations. In addition, localized "hot spots" may be anticipated in various operational circumstances.

In general, the actual determination of buckling conditions requires the employment of approximate methods of analysis and computation. However, the success of any approximate technique depends crucially on the selection of reasonable "shape functions" which reflect the buckled shape of the structure.

In this Note we consider an idealized, rotationally symmetric case which is amenable to an exact analytical solution. This solution offers a model for a suitable "shape function" and also provides an assessment for the circumstances under which thermal buckling may become a significant design factor.

Analysis

Consider a thin isotropic, elastic plate of thickness h and radius b, which is traction-free at $r = b$.

Let E, ν and α denote the Young's Modulus, Poisson's ratio and the coefficient of thermal expansion, respectively. The bending stiffness of the plate is given by $D = Eh^3/12(1-\nu^2)$. Let r denote the radial coordinate and consider the following temperature distribution

$$T(r) = T_o(1-r^2/b^2) + T_b \qquad (1)$$

*Professor, Mechanics & Materials Research Center, Civil Engineering Department, Texas A&M University, College Station, Texas, 77843.

Elementary computations [1] yield the following expression for the radial stress σ_r:

$$\sigma_r = \frac{1}{4} E\alpha\, T_o[-1+(r/b)^2] \tag{2}$$

Note that $\sigma_r < 0$ throughout the plate.

Let ϕ designate the slope of the buckled plate. Employing (2), we obtain the following expression for ϕ [2]:

$$r^2\phi'' + r\phi' - [(\frac{k}{b})^2 r^4 - k^2r^2 + 1]\,\phi = 0 \tag{3}$$

where $k^2 = \frac{E\alpha T_o h}{4D} = 3(1-\nu^2)\,\frac{\alpha T_o}{h^2}$, and primes designate derivatives with respect to r. It is interesting to note that (3) does not depend on Young's modulus. This is due to the fact that E contributes to both the stress σ_r and the stiffness D.

Introduce the new variables $\rho = r^2$, $z = \frac{k}{b}\rho$ and η.

Let $\phi(r) = \exp(-\frac{z}{2})\,\rho^{\frac{1}{2}}\,\eta(z)$. Subsitution into (3) gives

$$z\eta'' + (2-z)\eta' - (1 - \frac{kb}{4})\eta = 0 \tag{4}$$

where, in (4), primes indicate derivatives with respect to z.

Equation (4) is Kummer's equation [3] [4] which has, in general, two independent solutions. In the present case, one solution contains the term log z. This logarithmic solution is rejected because its leading term leads to the expression $\phi = A_2[r^{-1} \exp(-\frac{k}{2b} r^2) + \ldots.]$ which is singular at r = 0.

The remaining solution yields, after several straightforward manipulations

$$\phi = A_1\, x \exp(-\frac{kb}{2} x^2)\, U(1 - \frac{kb}{4}, 2, kbx^2) \tag{5}$$

In (5), $U(\alpha, \gamma, z) = \frac{\Gamma(\gamma)}{\Gamma(\alpha)} \sum_{n=0}^{\infty} \frac{\Gamma(\alpha+n)}{\Gamma(\gamma+n)}\,\frac{z^n}{n!}$

$x = r/b$ and A_1 is an arbitrary constant.

For a traction-free plate both bending moment M_r and shear force Q_r vanish at r = b. However, since $Q_r = N_r\phi = h\sigma_r\phi$ it follows from (2) that $Q_r(b) = 0$. The remaining condition, $M_r(b) = 0$, gives

$$\left[\frac{d\phi}{dr} + \frac{\nu}{r}\phi\right]_{r=b} = 0 \qquad (6)$$

Substitution of (5) into (6) yields, after several intermediate calculations, the following transcendental equation in λ

$$(1+\nu-\lambda)\, U(1 - \lambda/4,\, 2, \lambda) + \lambda(1-\lambda/4)\, U(2 - \lambda/4,\, 3, \lambda) = 0 \qquad (7)$$

where, in (7)

$$\lambda = kb = \sqrt{3(1-\nu^2)\alpha T_o}\ (b/h) \qquad (8)$$

The smallest non-zero root of (7) determines the critical temperature T_o which would cause thermal buckling. Substituting this value of $\lambda = kb$ into (5) we get the slope of the buckled shape $\phi = \frac{dW}{dx}$. The deflected shape W is obtained by numerical integration of (5).

Computations were performed with typical values for quasi-isotropic graphite/epoxy and glass/epoxy laminates, namely $\alpha = 7 \times 10^{-6}$ in/in/1°F, $\nu = 0.3$, and with $T_o = 20°F$. The smallest root of equation (7) was found to be $\lambda_{CR} = 2.405$. Substitution in (8) yields $\frac{b}{h} = 124.3$

It follows that unstiffened quasi-isotropic laminates with in-plane dimensions that exceed 100 times the thickness may be susceptible to thermal buckling if the non-uniformity in the temperature distribution exceeds 20°F.

A typical buckled shape is shown in Fig. 1, where the non-dimensionalized deflection w = W/b is plotted vs. the non-dimensional radial distance x = r/b. As in all buckling problems, the amplitude of the deflection remains indeterminate.

Acknowledgement

This investigation was conducted under Contract F-49620 78 C 0034 from the Air Force Office of Scientific Research (AF)SR). This support is gratefully acknowledged.

Figure Title

Shape of Deflection $w(x)$ vs. Dimensionless Distance $x = \frac{r}{b}$ with $\nu = 0.3$. The Critical Value of λ is $\lambda_{CR} = 2.405$.

References

[1] Timoshenko, S., and Goodier, J. N.: Theory of Elasticity, McGraw Hill, 2nd. Edition, 1951, p. 407.

[2] Timoshenko, S. P., and Gere, J. M.: Theory of Elastic Stability, McGraw-Hill, 2nd. Edition, 1961, pp. 389-391.

[3] Abramowitz, A., and Stegun, I. A. (Editors): Handbook of Mathematical Functions, U.S. Dept. of Commerce, National Bureau of Standards, Applied Mathematics Series No. 55, 1964, pp. 504-505.

[4] Magnus, W., Oberhettinger, F., and Soni, R. P.: Formulas and Theorems for the Special Functions of Mathematical Physics, Springer-Verlag, 3rd Edition, 1966, pp. 262-270.

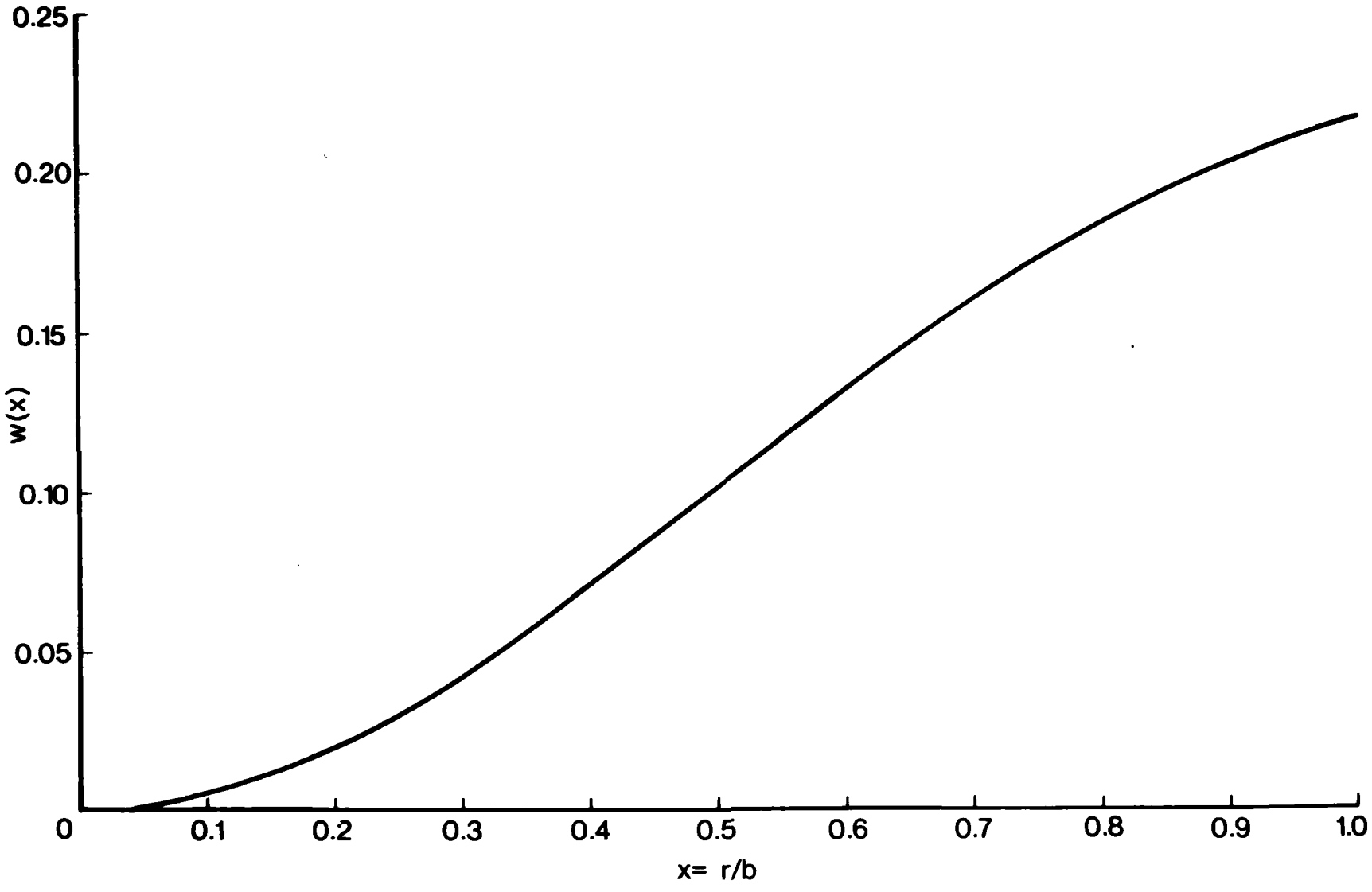
0.25
0.20
0.15
0.10
0.05
0
w(x)
0.1
0.2
0.3
0.4
0.5
0.6
0.7
0.8
0.9
1.0
x= r/b

A METHOD FOR DETERMINING THE MODE I DELAMINATION FRACTURE TOUGHNESS OF ELASTIC AND VISCOELASTIC COMPOSITE MATERIALS*

by

D. F. Devitt**, R. A. Schapery† and W. L. Bradley††

ABSTRACT

A method using a double cantilever, laminated beam specimen is developed to obtain delamination fracture toughness as a function of the rate of crack propagation. First, the relation between energy release rate, applied displacement, and various laminate parameters is derived using a large displacement, small strain theory. Experiments employing unidirectional glass/epoxy composites of three different thicknesses and a wide range of loading rates are then described. Although the beam deflections and rotations are very large, good agreement between measured and predicted beam compliance is demonstrated. The energy release rate G_c and crack speed $\dot{L}$ are shown to obey the power law $G_c \sim \dot{L}^{0.1}$; essentially the same result is obtained for all three laminate thicknesses.

---

* To be submitted for publication

** Structures Engineer, Vought Corporation, Dallas, Texas

† Professor of Civil and Aerospace Engineering
Texas A&M University, College Station, Texas 77843

†† Professor of Mechanical Engineering
Texas A&M University, College Station, Texas 77843

INTRODUCTION

Predictions of the useful life for composite material components require a comprehensive understanding of the materials response to complex load histories in anticipated service environments in the presence of defects such as microcracks, voids, and delaminations. Such defects can occur during manufacturing or may develop in service, causing structural degradation or failures at stresses well below the strength levels expected for defect free material. Linear elastic fracture mechanics (LEFM) has been developed to deal with crack-like defects by relating defect geometry and design stress to a material response, normally called the fracture toughness of the material. The fracture toughness of a material is usually characterized by critical energy release rate (G_c) or the critical stress intensity K_c.

In an ideal monolithic isotropic material the fracture toughness is independent of the orientation of the crack plane for a given mode of deformation at the crack tip, such as the opening mode. However, in an anisotropic composite material, the material response may vary considerably depending on the plane of fracture and the energy dissipative processes involved. Work to date has indicated toughness values of 14-28 ksi$\sqrt{in}$ for center notched tensile specimens of fiber-reinforced plastic laminates [1], which compare favorably with aluminum alloys often used in the aircraft industry which have K_{1c} values of 21-40 ksi$\sqrt{in}$ [2].

Growth of interlaminar flaws (delamination) is an important part

of the failure process in many laminates [3, 4]. Compressive fatigue appears to be an especially severe type of loading in producing delaminations [5, 6]; out of plane stresses developed through compressive loading and local buckling are thought to be the primary cause of such delamination type fractures. These observations indicate that the delamination fracture toughness may be the critical toughness parameter for fatigue stressing where the minimum stresses are compressive.

While considerable effort has been expended to define fracture toughness for tensile loading of laminates with flaws normal to lamina planes, very little has been done to better define and understand the delamination fracture behavior. Apparently, the few studies that have been conducted to characterize delamination have utilized specimen geometries that give a mixed tensile and shear stress state at the delamination crack tip [3, 7, 8] (see Figure 1a): precluded, therefore, is determination of K_{1c} or G_{1c} for the opening mode of delamination in which only tensile stresses exist at the crack tip. In order to fully characterize delamination fracture toughness we believe it is necessary to study the effect of various proportions of tensile and shearing stresses at the crack tip, including the opening mode.

The objective of the investigation described herein has been to develop an experimental approach with the associated analysis to obtain the critical energy release rate for the opening mode of delamination. A double cantilever beam geometry was chosen to give essentially pure opening mode fracture (Figure 1b). To allow the study of thin laminates, nonlinear beam theory was used in the analysis. Experimental measurements were made on Scotchply (a composite consisting of epoxy

matrix reinforced with continuous glass fibers) to verify the analysis and allow determination of the delamination fracture toughness of this material. The analytical approach will be presented in the next section, followed by a description of the experimental program. The results, including raw data and reduced data will then be presented with appropriated discussion, from which final conclusions will be drawn.

The thin, double cantilever beam geometry gives rise to stable crack growth, and therefore is particularly suited to determine the relation between slow crack speed and the fracture toughness. A portion of our study therefore has been devoted to characterizing delamination growth rate in terms of energy release rate.

ANALYTICAL PROCEDURES

Consider the beam specimen in Figure 1b, in which the delamination crack tip is at the point x = a. The energy release rate associated with a virtual crack growth of an amount da is, by definition, the mechanical energy that becomes available at the crack tip per unit area of new surface. In terms of the total strain energy in an elastic beam, W, this release rate is

$$G = -\frac{1}{B}\frac{\partial W}{\partial a} \tag{1}$$

where the derivative is evaluated for constant beam tip displacement Δ. Also, B is specimen width normal to the page. The value of G at which the crack actually starts to propagate is the critical energy release rate or fracture toughness, G_c.

Evaluation of Equation (1) for our specimen geometry (Figure 2)

requires determination of the strain energy stored in the double cantilevered beam as a function of the parameters of grip displacement (Δ), moment arm L-d, moment of inertia I, and the modulus of elasticity, E, in the length direction of the beam. The calculation of the strain energy stored in a nonlinear beam in terms of these parameters will be presented next.

Strain Energy in a Nonlinear Beam

The strain energy in a cantilever beam under a concentrated end load is found from elementary beam theory to be,

$$W_1 = \frac{1}{2} \int_0^L \frac{M^2}{EI} \, ds \tag{2}$$

where M is the bending moment, E is the axial modulus of elasticity, I is the area moment of inertia, and L is the underformed beam length.

As a result of the low flexural rigidity of thin composite specimens, large deflections and rotations may be present during the test and need to be accounted for in the analysis. Such a correction to linear beam theory has been made by Bisshopp and Drucker [10], where they included the square of the rotation in the strain-displacement relation and the effect of the beam shortening of the moment arm due to large deflections. A linear stress-strain equation and small strains were assumed.

The nomenclature and geometric relationships used by Bisshopp and Drucker are shown in Figure 2. The principal results of their analysis are:

$$\left(\frac{PL^2}{EI}\right)^{\frac{1}{2}} = \frac{\sqrt{2}}{2} \int_0^{\phi_0} (\sin\phi_0 - \sin\phi)\, d\phi \tag{3}$$

$$\Delta = \left(\frac{EI}{2P}\right)^{\frac{1}{2}} \int_0^{\phi_0} \frac{\sin\phi}{(\sin\phi_0 - \sin\phi)^{1/2}}\, d\phi \tag{4}$$

where ϕ_0 is the angle of slope at the loaded end of the beam, ϕ is the slope of the beam at intermediate points, P is the load, and the remaining terms were defined previously. After determining the appropriate change of variables and transformations Bisshopp and Drucker were able to rearrange Equations (3) and (4) into canonical elliptic form as shown below:

$$\left(\frac{PL^2}{EI}\right)^{1/2} = F(k) - F(k, \phi) \tag{5}$$

and

$$\frac{\Delta}{L} = 1 - 2\left(\frac{E(k) - E(k, \phi)}{F(k) - F(k, \phi)}\right) \tag{6}$$

where F(k) and E(k) are the complete elliptic integrals of the first and second kind respectively, $F(k, \phi)$ and $E(k, \phi)$ are incomplete elliptic integrals of the second kind, and k and ϕ are elliptic parameters [11]. Since the results for $\frac{\Delta}{L}$ and $\left(\frac{PL^2}{EI}\right)^{1/2}$ are single-valued functions of the same elliptic parameters, they are implicitly related through Equations (5) and (6), with relationship presented in Table 1 and Figure 3.

Next, the strain energy stored in the two cantilevered beams must be calculated. Combining the general definition for strain energy W_1 in a beam (Equation 2) with the specific result from non-linear beam analysis (Equation 3), one may express the total strain energy $W = 2W_1$ in terms of elliptical integrals as follows:

$$\frac{WL}{2EI} = (F(k) - F(k, \phi))^2 \left(\frac{E(k) - E(k, \phi)}{F(k) - F(k, \phi)} + 2(k^2 - 1) \right) \quad (7)$$

The results of such a calculation are presented in Figure 4 and Table 1. Next, the energy release rate as defined in Equation 1 will be evaluated using the strain energy for a nonlinear beam as calculated in Equation 8.

Energy Release Rate (G) for a Nonlinear Beam

It is clear from Figure 4 that increasing the load (or grip) displacement "Δ" for a fixed crack length "L" will increase the strain energy stored in the specimen, "W". From the same Figure 4 it is also clear that crack extension (increasing L) which occurs at constant grip displacement (Δ) results in a decrease in the strain energy (W) stored in the specimen, as shown schematically in Figure 5. As the specimen with length (or crack size) L_1 is loaded from Δ_1 to Δ_2, the strain energy W is seen to increase. The strain energy release rate

$$G_\Delta \equiv -\frac{\Delta W}{B\Delta L} \quad (8)$$

is also seen to increase as the test goes from a-b. Suppose at "b" the critical energy release rate is achieved and crack extension occurs, changing the crack length from L_1 to L_2. At point "c" the energy release rate is again insufficient to give crack extension, so that further loading to point "d" is necessary, which again corresponds to G equal to the critical energy release rate. Crack extension occurs from L_2 to L_3 as one moves along d-e. In an actual test the loading and crack extension occur more or less continuously, instead of in steps. Indeed the

energy release rate may be calculated as $-\frac{1}{B}\frac{\partial W}{\partial L}$ for constant Δ. The path a-c-e for $G = G_c$ represented by the dotted line in Figure 5 would be followed in an actual experiment.

The present theoretical prediction of G can be used for viscoelastic materials if the axial stress-strain relation is elastic; this is a good approximation for our tests since we have employed only unidirectional laminates with fibers parallel to the beam axis. However, the resin has a significant influence on the energy absorbed at the crack tip, and therefore the beam will be locally viscoelastic. Consequently, crack growth rate $\dot{L}$ depends on the stress intensity factor, K_I and therefore on the critical energy release rate [12]. For the usual case in which $dL/dG > 0$, a slower crosshead speed results in a slower crack growth rate; thus, a different path with smaller values of G would be traversed as shown by the dotted line in Figure 5.

Since $\frac{WL}{EI}$ is a single-valued function of Δ/L, as seen in Figure 4, one may write

$$\frac{WL}{2EI} = f(\Delta/L) \tag{9}$$

Differentiation of "W" at constant Δ gives

$$\frac{1}{2}\frac{\partial W}{\partial L}\bigg|_{\Delta} = -\frac{EI}{L^2}\left[f\left(\frac{\Delta}{L}\right) + \frac{\Delta}{L}\,\frac{\partial f(\Delta/L)}{\partial(\Delta/L)}\right] \tag{10}$$

Next, define $\bar{S}$,

$$\bar{S} \equiv d\ \log(WL/EI)/d\ \log(\Delta/L) \tag{11}$$

Therefore, from Equations (9) - (11),

$$G = -\frac{\partial W}{B\partial L} = \frac{EI}{BL^2}\left(\frac{WL}{EI}\right)\quad(1 + \bar{S}) \tag{12}$$

The logarithmic slope $\bar{S}$ is drawn in Figure 6.

A rearrangement of Equation 12 yields a nondimensional form of the energy release rate for one of the two beams,

$$\frac{1}{2}\frac{GBL^2}{EI} = \frac{1}{2}\frac{WL}{EI}(1 + \bar{S}) \tag{13}$$

Since both WL/EI and $\bar{S}$ in Equation 13 are functions of Δ/L, GBL^2/EI is an implicit function of Δ/L. Using Equation 13 in conjunction with Figures 4 and 6, GBL^2/EI as a function of Δ/L has been evaluated and presented graphically in Figure 7. Suppose that during quasi-static crack growth, one determines Δ/L at any given time in a delimination fracture test: Figure 7 then allows one to determine G_c directly as $G_c = G$ for a growing crack.

In summary, the relationshops between Δ/L and P, W and G have been determined in terms of elliptical integrals using nonlinear beam analysis. These results are summarized in Figures 3, 4 and 7 and Table 1 and will be used to analyze the experimental results to be described in the next section.

EXPERIMENTAL PROCEDURES AND RESULTS

The experimental program to be described in this section had two objectives: (1) to experimentally verify the nonlinear beam analysis; and (2) to measure the critical energy release rate as a function of crack growth rate, as suggested by Schapery [12]. In this section, specimen preparation and testing will be described, typical raw data will be presented, and reduction of the data to critical energy release

rate values (G_c) using the previously described nonlinear beam analysis will be detailed. Finally, a summary of all of the results will be presented in tabular and graphical form.

Specimen Preparation

Scotchply, which is an E-glass reinforced type 1003 epoxy, was selected for this study because it is translucent, which makes the visual measurement of the moving crack front during testing quite easy. Eight, twelve, and sixteen ply 12" x 12" panels were laid up using prepreg tape containing continuous fiberglass filaments. All lamina had the same fiber orientation in the laminates. After curing, the 12" square laminates were cut parallel to the fiber direction into one inch wide unidirectional test strips. The cured lamina thickness is about .00832 inches, giving laminate thicknesses of 0.067, 0.102 and 0.133 inches, respectively, for the 8, 12 and 16 ply specimens.

Test Procedure

The specimens were tested in an ambient environment (approximately 75°F and 50% RH) using an Instron tensile test machine with a one thousand pound load cell; a twenty pound full scale range was used. Special grips were designed to allow the load to be applied along a fixed line of action while permitting a virtually free rotation of the loaded ends of the double cantilever beam, as was assumed in the analysis (see Figure 2). Load was monitored as a function of time using a strip chart recorder. The displacement versus time was calculated from

the crosshead speed. The crack position as a function of time was noted visually as the crack front passed reference marks on the specimens. A specimen test in progress is shown in Figure 8. Typical experimental results are presented in Table 2 for a twelve ply specimen tested at a crosshead speed of 1 inch/minute. Five each of the eight, twelve and sixteen ply specimens were tested at a crosshead speed at one inch/minute. One specimen was tested with a crosshead speed that varried from .01 inch/minute to 10 inch/minute.

Data Reduction

The measured data included load (P), grip displacement (2Δ), and crack length (l); they can be easily reduced to give the critical energy release rate (G_c) using the analysis described in an earlier section, especially the results of that analysis tabulated in Table 1. After determining Δ/L, Lagrangian interpolation was used to calculate PL^2/EI, WL/EI, and $\bar{S}$. The results of these interpolations, along with the subsequent calculation of the critical energy release rate G_c using Equation 13, are summarized in Table 2. The crack growth rate was calculated from the measured values of grip displacement versus crack extension (L), knowing the rate of grip displacement. From the measured values of P, 2Δ, and L, the effective flexural rigidity term was determined.

Experimental Results

Results taken from 8, 12, and 16 ply specimens have been superimposed on Figure 4, as seen in Figure 9. While $\frac{PL^2}{EI}$ can be predicted directly by

the analysis as shown by the solid line, the values may also be determined directly from measured quantities. The accuracy of the analysis is clearly demonstrated by the fact that the experimental data points for all three specimen thickness fall nicely on the curve predicted from the analysis. Another way of demonstrating the accuracy of the analysis is to predict the crack length L at various times in a test using the measured values of P and 2Δ. The predicted values are compared with the experimental values in Table 3 for a twelve ply specimen. The agreement is seen to be excellent.

The critical energy release rate results are presented graphically in Figure 10 as a function of crack growth rate, $\dot{L}$. As expected, higher crack growth rates required larger critical energy release rates. Furthermore, the sixteen ply specimens had a higher G_c value than did the eight ply specimen, though only slightly. The modulus of elasticity values determined in the analysis indicated values of 6.35×10^6, and 4.95×10^6 psi for the 8,12, and 16 ply specimens. This variation seems to reflect a decreasing fiber volume fraction with laminate thickness, which was subsequently confirmed using density measurements. This type of variation is reasonable as it is more difficult to bleed out the excess resin in the thicker laminates, giving them a higher volume fraction of residual resin, and therefore, a lower modulus of elasticity. The higher G_c values observed for the thicker laminates also suggest that a greater volume fraction of resin may slightly enhance the fracture toughness. Photomicrographs of the three specimens are shown in Figures 11a-11d. The fiber distribution in all three specimens is seen to be heterogeneous, and in many cases the fibers appear to be in contact.

DISCUSSION

The measured critical energy release rates are seen to have a definite crack growth rate dependence. Schapery [12] has predicted that crack growth rates in viscoelastic material may be described by an equation of the form

$$\frac{dL}{dt} = c_1 G_c^{\left(1 + \frac{1}{n}\right)} \tag{14}$$

if the intrinsic fracture energy and strength are independent of crack speed. The exponent depends on n, which is a material constant that describes the resin creep complaince D(t) through an equation of the form $D = D_0 + D_1 t^n$. The value of n = 0.1 is obtained from Figure 2 and Equation (14). In order to check this value, creep/recovery tests were run on 90° (fiber angle) specimens of Scotchply to determine the time dependence of the matrix. An exponent of n = 0.05 - 0.10 was determined for these tests, which is consistent with the fracture results for delamination fracture toughness.

Delamination fracture toughness of Scotchply has been measured by Wu [13] using a center-notched specimen with 90° fibers. He obtained a value of 1.75 Ksi$\sqrt{\text{in}}$ for K_c. These results may be compared to our results if our measure d_c values are expressed in terms of K_c using the relationship

$$K_{1c} = (\hat{E}G)^{\frac{1}{2}}$$

where E is the effective modulus and has been shown to be approximately equal to one half the transverse modulus E_{22} for an orthotropic material [12].

Utilizing the manufacturer's predicted value for E_{22} of 1.4×10^6 psi and the observed range of G_c values of 3.0 - 5.5 lbs/in. gives a predicted range of values for K_c of 1.5 - 2.0 ksi$\sqrt{in}$, in good agreement with Wu's results. These values may also be compared with values measured for metals and other plastics, as summarized in Table 4.

Several assumptions were made implicitly in the analysis that appear to be justified by the good agreement between the predictions and measurements for the nonlinear beam analysis, as seen in Figure 9. These assumptions include plane stress and "rigid wall" behavior at beam end point, which in our specimen is the crack front. The actual behavior in this region may only be described by a more complex three dimensional analysis using finite elements; however, the departure from rigid wall behavior appears to have a sufficiently small effect on the overall strain energy stored in that it may effectively be neglected. Fiber breakage in the other fibers could also have introduced an error into the strain energy calculations as well as the measured critical energy release rate. Simple calculations indicate that the axial stress in the beam never reached the failure value; furthermore, almost no fiber fracture was noted in the tests. Finally, as a result of transverse strains (normal to the loading direction), the beam has a compound curvature which would tend to stiffen the beam and depend on beam length. Again, in view of the agreement in Figure 9, this effect was apparently neglible for the specimens used.

CONCLUSION

A new approach to the determination of delamination fracture toughness in the opening mode has been developed using a double cantilever beam with a nonlinear beam analysis. The analysis has been confirmed with experimental measurements on Scotchply using specimens of three thicknesses, tested over a wide range of crack growth rates. The measured critical energy release rate of 3.0 - 5.5 lbs/in for the range of crack growth rates studies has been analyzed using viscoelastic crack growth rate theory and found to give results consistent with the viscoelastic behavior of the resin as determined from creep/recovery tests.

ACKNOWLEDGMENT

This research was sponsored by the Air Force Office of Scientific Research under contract No. F49620-78-C-0034 with Texas A&M University.

The authors are indebted to Professor K. L. Jerina for his valuable guidance in the experimental phase of the study and to Mr. R. C. Hulsey for his very able assistance in conducting tests during the latter stages of the work and for making the photomicrographs in Figure 11.

REFERENCES

1. Kausch, H.H., Polymer Fracture, Springer-Verlag, Berlin, 1978, p. 256.

2. Hertzber, R.W., Deformation and Fracture Mechanics of Engineering Materials, Wiley, New York, 1976, p. 285.

3. Kulkarni, S.V., Pipes, R.B., Ramkumar, R.L., Scott, W.R., " The Analytical, Experimental, and Nondestructive Evaluation of the Criticality of an Interlaminar Defect in a Composite Laminate", Proceedings of the 1978 International Conference on Composite Materials, Toronto, 1978, pp. 1057-1071.

4. Reifsnider, K.L., "Mechanics of Failure of Composite Materials," In Fracture Mechanics, Proc. 10th Symposium on Naval Structural Mechanics, Univ. Press of Virginia., 1978, pp. 317-331.

5. Grimes, G.C., and Adams, D.F., "Investigation of Compression Fatigue Properties of Advanced Composites", Northrop Technical Report, NOR 79-17, Dept. of the Navy, NASC Contracts N00019-77-C-0518 and N00019-77-C-0519 with Northrop and the University of Wyoming, October 1979.

6. Wilkins, Dick, General Dynamics, Fort Worth, Texas, private communication.

7. Wang, S.S. and Mandell, J.F., "Analysis of Delamination in Unidirectional and Crossplied Fiber-Composites Containing Surface Cracks", NASA Technical Report NASA-CR-135248, May 1977.

8. Wang, S.S., "Delamination Crack Growth in Unidirectional Fiber-Reinforced Composites Under Static and Cyclic Loading", ASTM Symposium on Composite Materials—Testing and Design, March 20, 1978, New Orleans, Louisiana.

9. Hertzberg, R.W., Deformation and Fracture Mechanics of Engineering Materials, Wiley, New York, 1976, p. 260.

10. Bisshopp, K.E., and Drucker, D.C., "Large Deflection of Cantilever Beams", Quarterly of Applied Math, Vol. III, 1945, p. 272.

11. Selby, Samuel M. (Editor in Chief), Standard Mathematical Tables, 19th Edition, The Chemical Rubber Co., Cleveland, Ohio, July 1971.

12. Schapery, R.A., "The Relation Between Energy Release Rate and Stress Intensity Factors for Orthotropic Viscoelastic Materials", in preparation.

REFERENCES (continued)

13. Wu, E.M., "Fracture Mechanics of Anisotropic Plates", Progress in Materials Science, Vol. I, 1968, Technomics, Stanford, Connecticut, p. 20.

Table 1. Nonlinear Variables

θ	k	α	$\frac{PL^2}{EI}$	$\frac{\Delta}{L}$	$\frac{WL}{2EI}$
45	.7071	0	0	0	0
50	.7660	.5942	.3530	.1161	.0203
55	.8192	.8547	.7305	.2301	.0819
60	.8660	1.0782	1.1625	.3404	.1855
65	.9063	1.3009	1.6923	.4455	.3339
70	.9397	1.5467	2.3922	.5437	.5318
75	.9659	1.8454	3.4057	.6340	.7901
80	.9848	2.2542	5.0813	.7167	1.1326
85	.9962	2.9459	8.6780	.7948	1.6488
88	.9994	3.8606	14.9040	.8472	2.2416
90	1.0000	∞	∞	1.0000	∞

Table 2. Experimentally Measured Values of Crack Length (L), Load (P) and Grip Displacement (2Δ) for Twelve Ply Sepcimen. Also Tabulated are Various Intermediate Terms Calculated in Determining G_c from the Experimentally Measured Terms.

L (in)	2Δ (in)	(lbs)	Δ/L	PL^2/EI	$\frac{WL}{EI}$	S	G_c lbs/in
3.5	2.22	6.07	.317	1.0681	.1596	2.1238	5.65
4.0	2.85	5.48	.3563	1.2307	.2045	2.1560	5.73
4.5	3.61	4.97	.4011	1.4446	.2644	2.1919	5.79
5.0	4.37	4.62	.4370	1.6420	.3198	2.2338	5.80
5.5	5.14	4.25	.4672	1.8270	.3719	2.2824	5.66
6.0	5.96	3.99	.4967	2.0259	.4285	2.3410	5.62
6.5	6.92	3.81	.5323	2.2965	.5051	2.4231	5.72
7.0	7.80	3.67	.5571	2.5116	.5647	2.4866	5.73
7.5	8.83	3.54	.5887	2.8296	.6491	2.5761	5.79
8.0	9.71	3.33	.6069	3.0414	.7027	2.6342	5.58
8.5	10.58	3.17	.6224	3.2418	.7515	2.6892	5.41
9.0	11.38	2.91	.6322	3.3794	.7840	2.7272	5.02
9.5	12.64	2.97	.6653	3.9188	.9044	2.8809	5.30
10.0	13.81	3.01	.6905	4.4269	1.0089	3.0321	5.52

Table 3. Comparison of Measured Values of Crack Length (L) To Value Calculated Using Nonlinear Beam Analysis and Measured Values of Grip Displacement (2Δ) and Load (P).

Measured Crack Length (in.)	Calculated Crack Length (in.)
3.50	3.51
4.00	3.99
4.50	4.52
5.00	5.00
5.50	5.50
6.00	5.99
6.50	6.51
7.00	6.97
7.50	7.50
8.00	8.01
8.50	8.49
9.00	9.02
9.50	9.55
10.00	10.06

Table 4. Typical Fracture Toughness Parameters (K_{IC} and G_c)

Material	K_{IC} ($ksi\sqrt{in}$)	G_c (lbs/in)
Metals [5, 10]		
Ti-6Al-4V	105	689
7075-T651	22	47
4340	55 - 90	104 - 279
2024 T3	40	152
Thermoplastic Materials [11, 12]		
Polymethyl Methacrylate	1.46 - 1.74	6.05
Polystyrene	.894 - 1.00	2.0
Polyvinyl Chloride	1.45 - 2.05	7.024
Nylon - 6, 6	.462 - .756	1.428
Polyethylene	.756 - 1.069	28.5

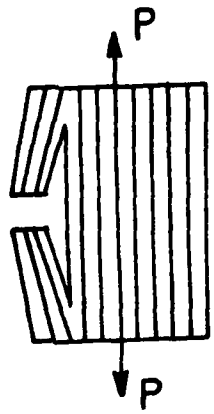

Figure 1a. Wang/Mandell specimen for delamination fracture toughness studies

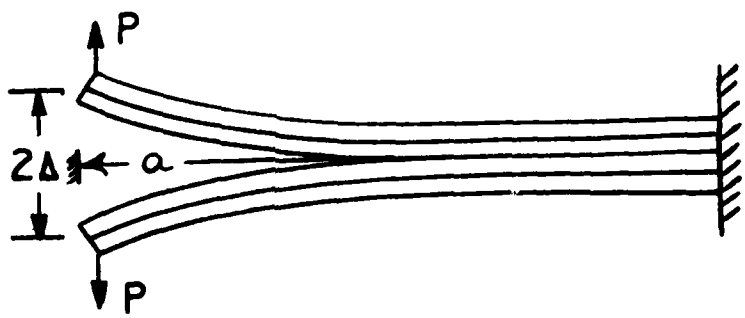

Figure 1b. Double cantilever beam specimen used in this work for delamination fracture toughness studies

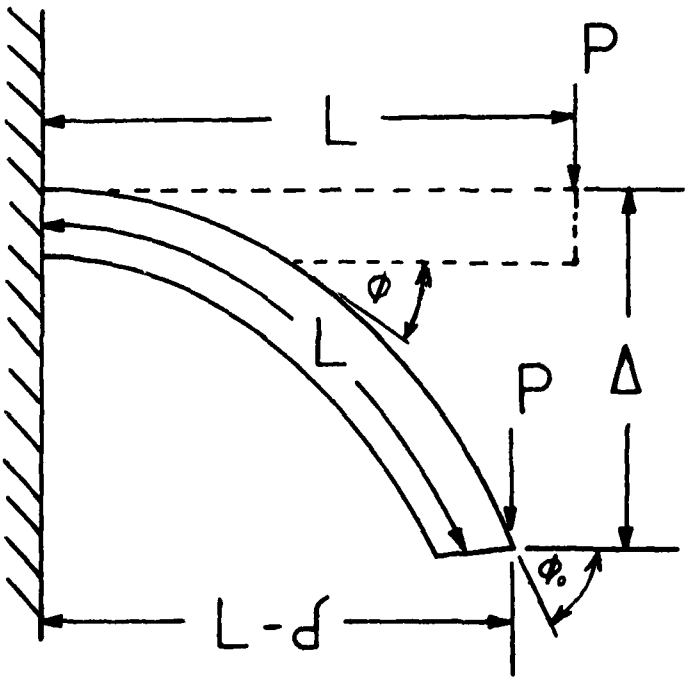

Figure 2. Cantilever beam nomenclature used in nonlinear beam analysis

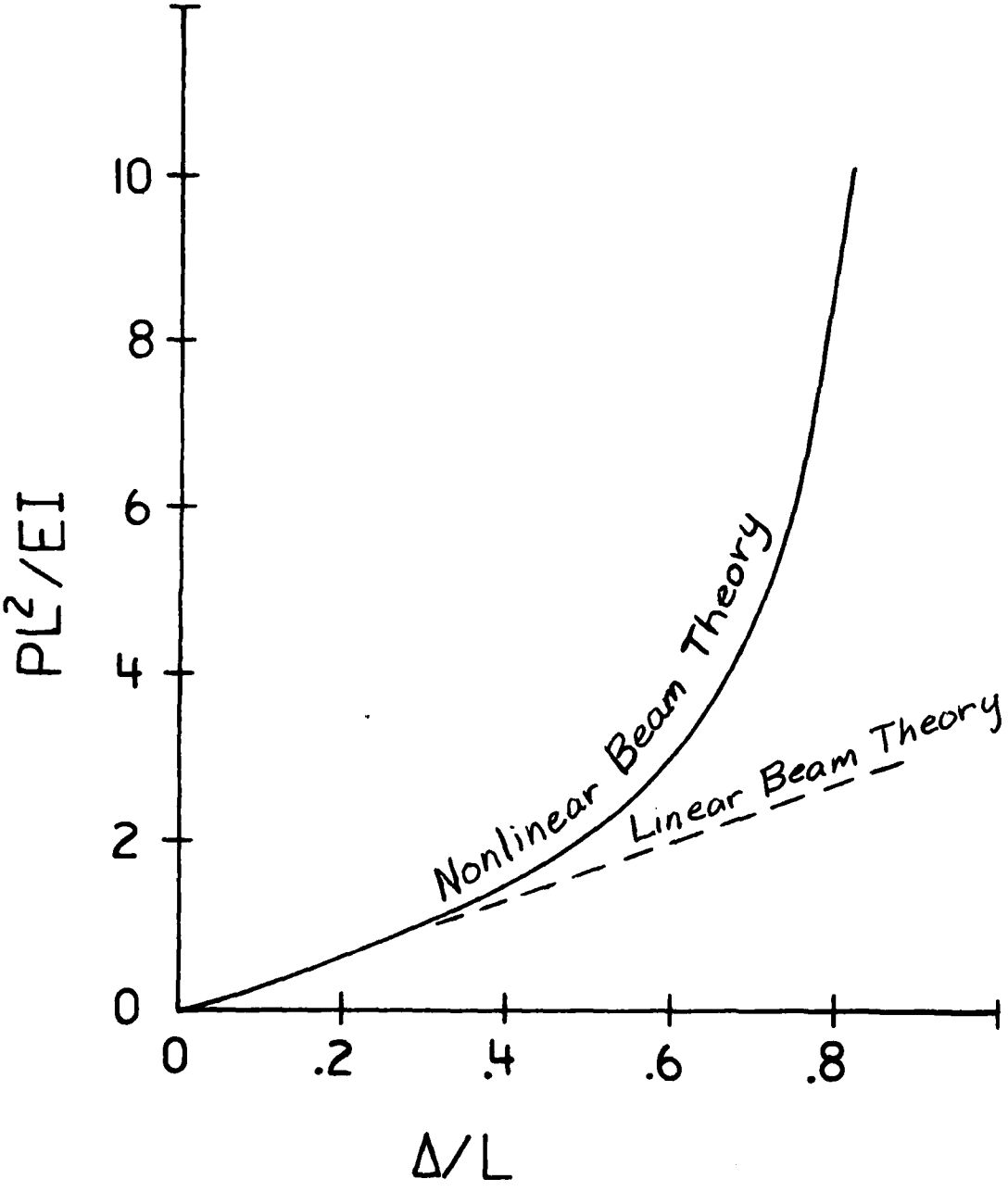

Figure 3. (PL^2/EI) vs. (Δ/L) as determined from nonlinear beam analysis

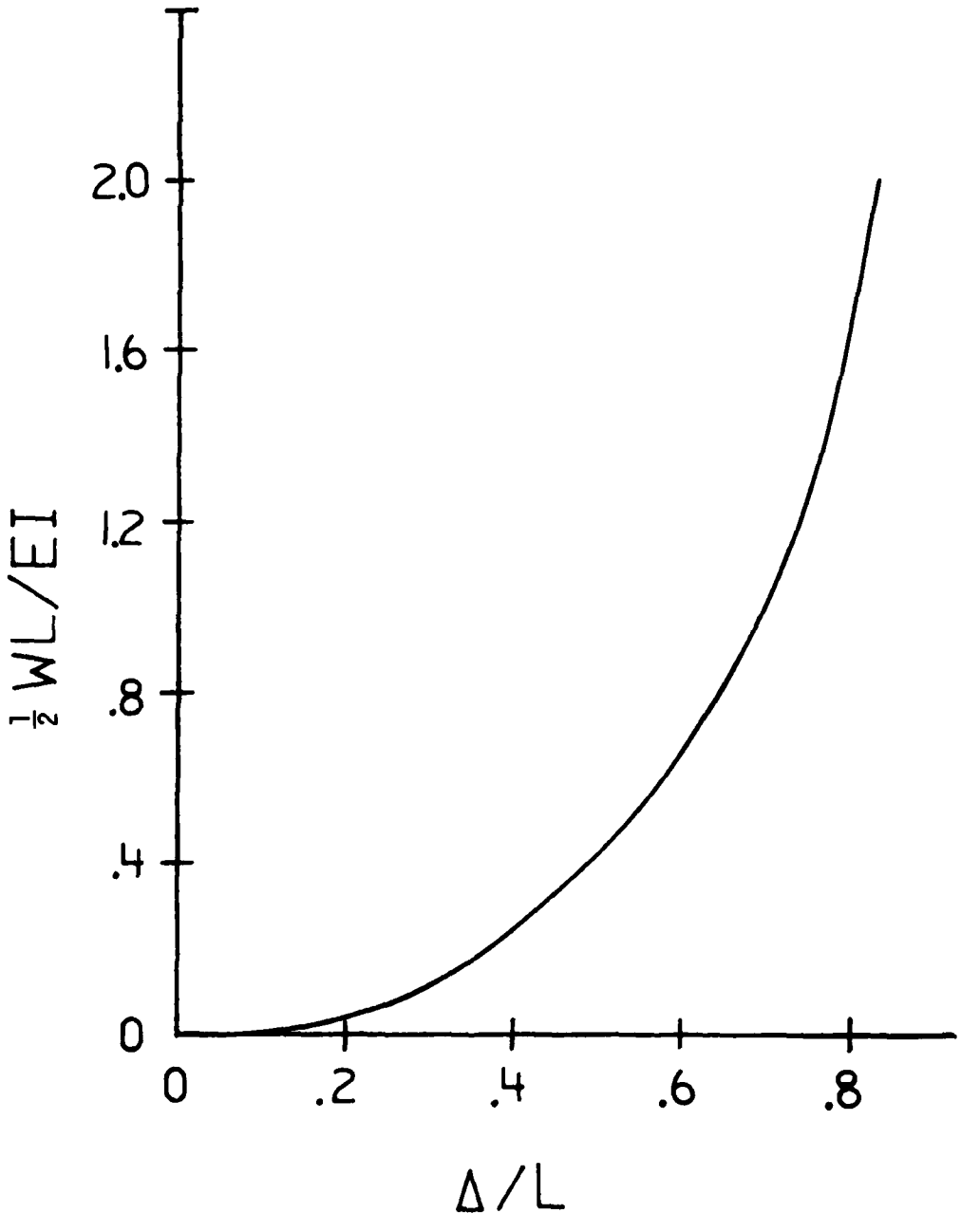

Figure 4. (WL/2EI) vs. (Δ/L) as determined from nonlinear beam analysis

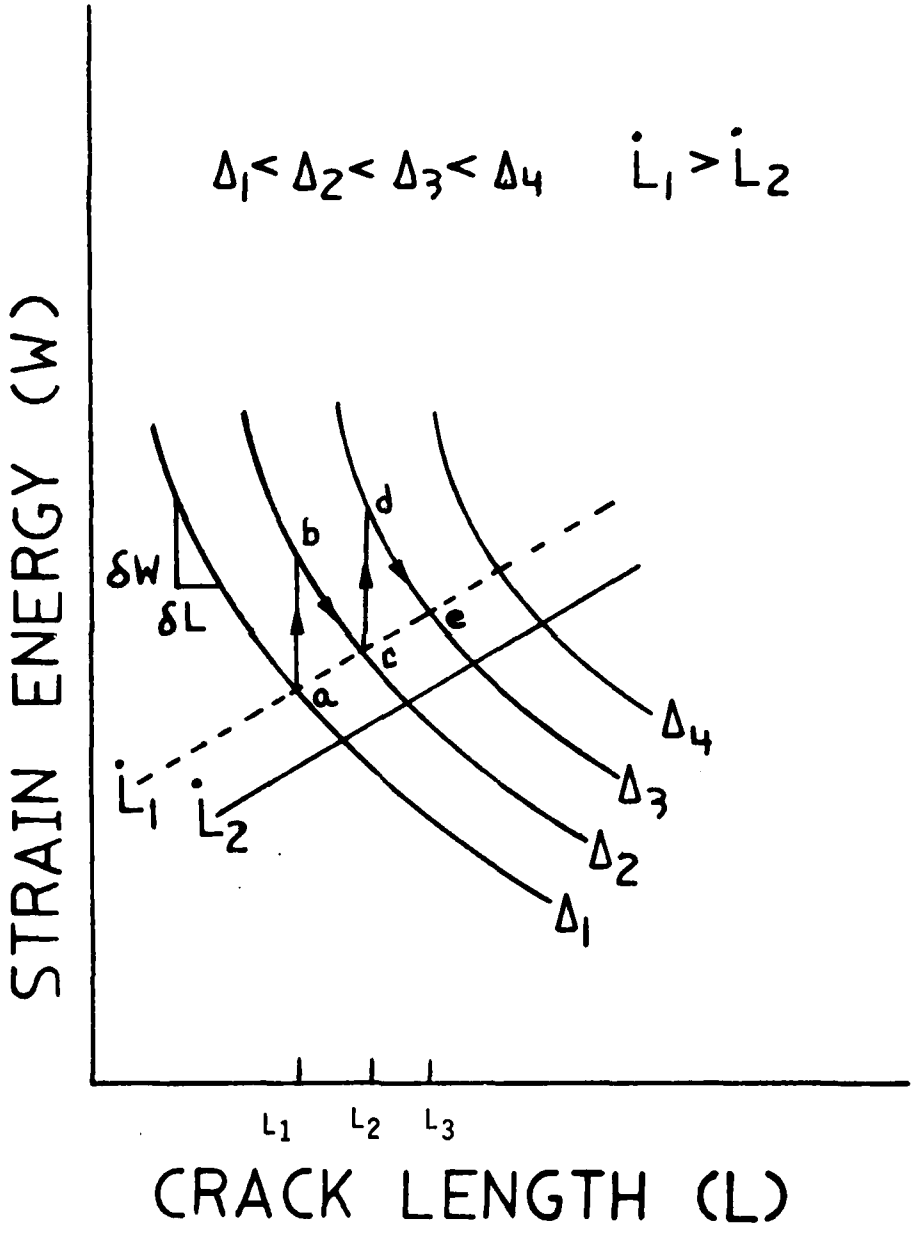

Figure 5. Schematic illustrating strain energy vs. crack length for several grip displacements, Δ

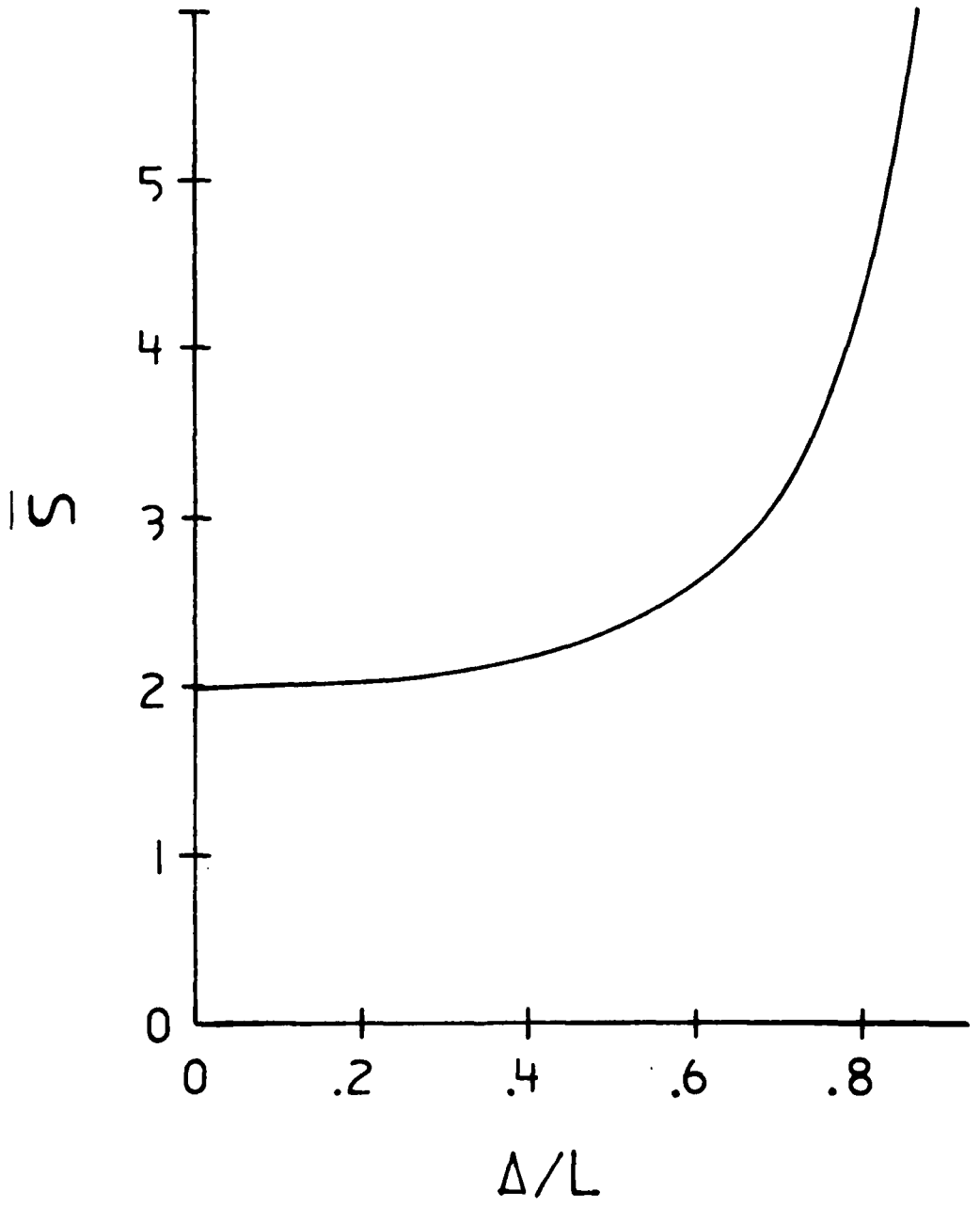

Figure 6. Dependence of logarithmic slope $\bar{S}$ (Equation 11) on beam deflection

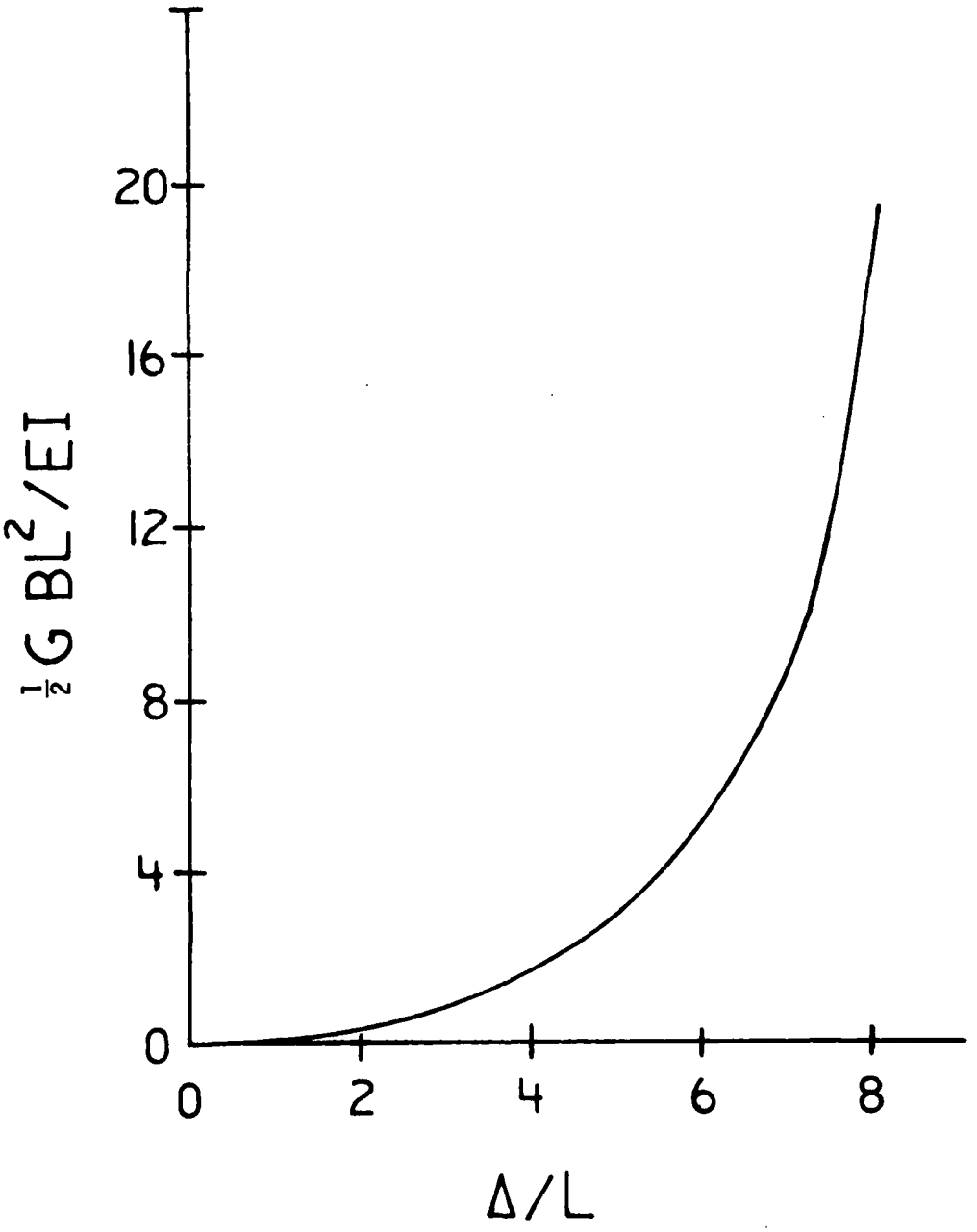

Figure 7. Nondimensional energy release rate as calculated from nonlinear beam analysis

Figure 8. Double cantilever beam test sequence.

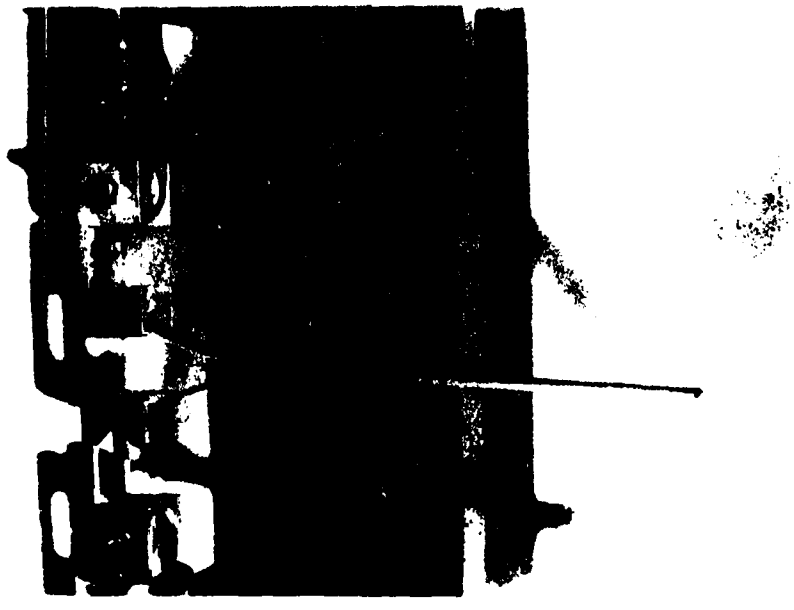

Figure 8. (continued)

Figure 8. (continued)

Figure 8. (continued)

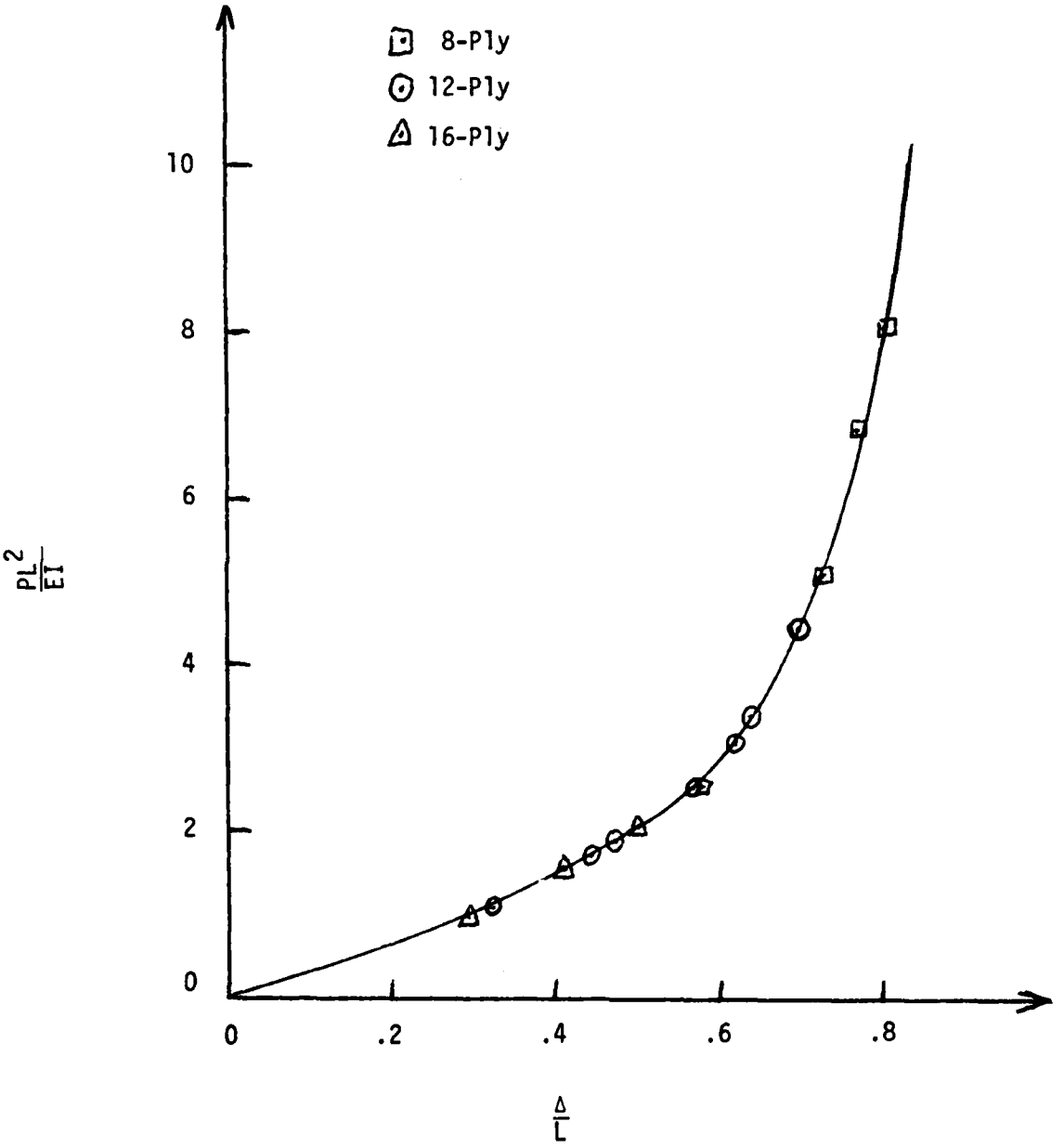

Figure 9. Verification of nonlinear beam analysis (solid line) with data points determined from measurement of P, L, E and Δ

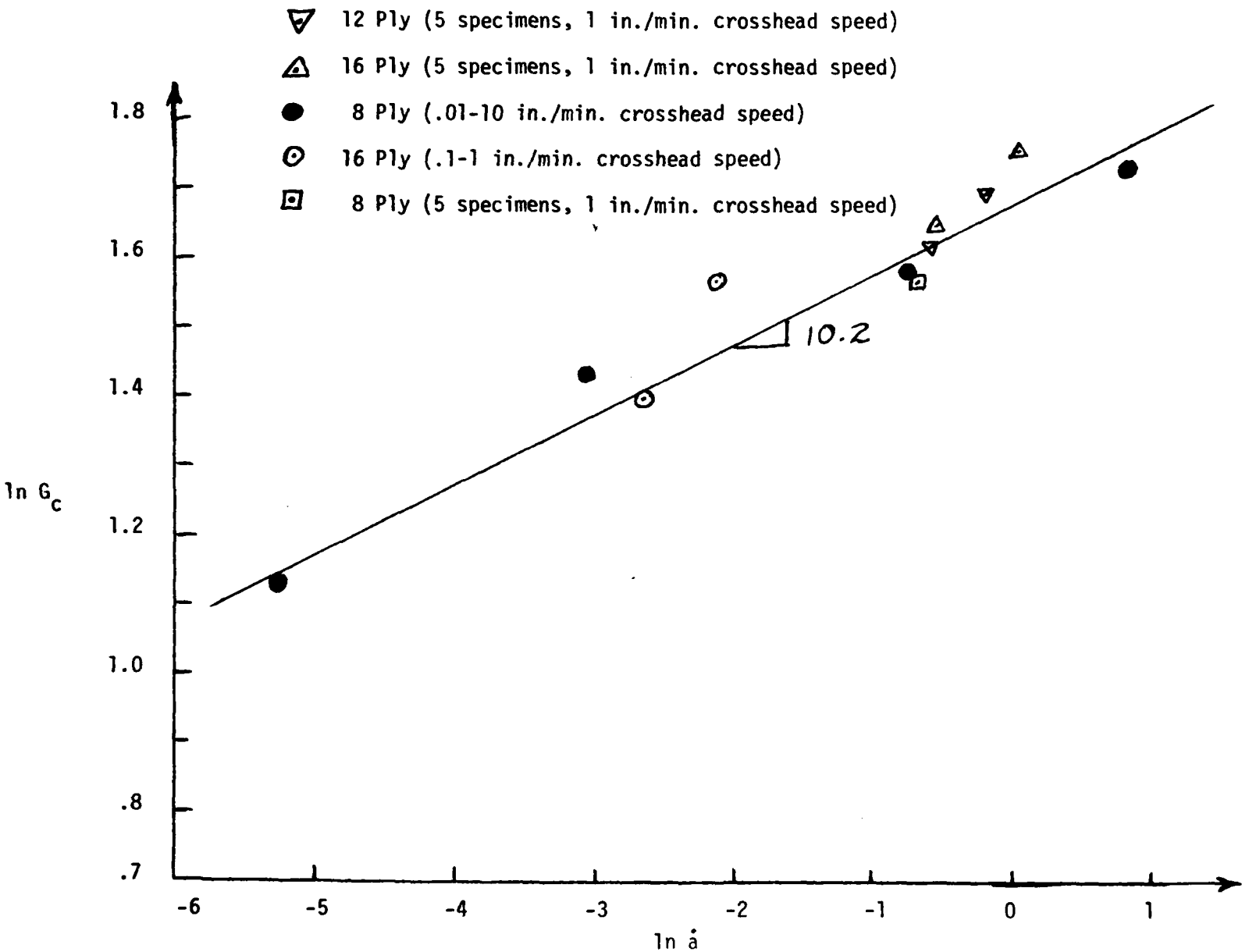

Figure 10. Calculated critical energy release rate G_c for various crack growth rates $\dot{a}$ and ply thickness in delamination fracture of Scotchply

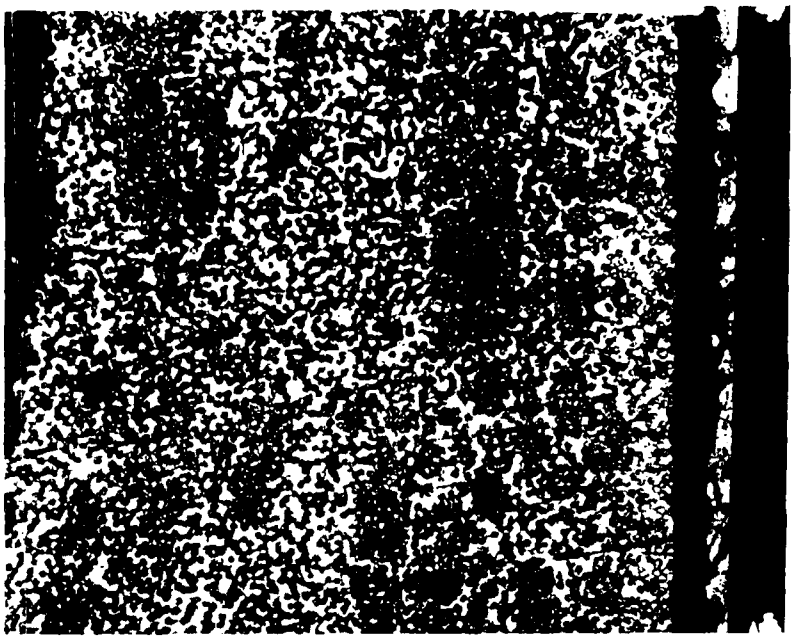

(a) 8 ply specimen, 100x.

(b) 12 ply specimen, 500x.

Figures 11a-11d. Photomicrographs of Scotchply showing distribution of glass fibers in epoxy matrix.

AD-A083 721 TEXAS A AND M UNIV COLLEGE STATION MECHANICS AND MAT--ETC F/G 11/4
COMPOSITE MATERIALS FOR STRUCTURAL DESIGN.(U)
FEB 80 R A SCHPEY F49620-78-C-0034
UNCLASSIFIED MM-3724-80-1 AFOSR-TR-80-0307 NL

2 OF 2


OF
2
83721

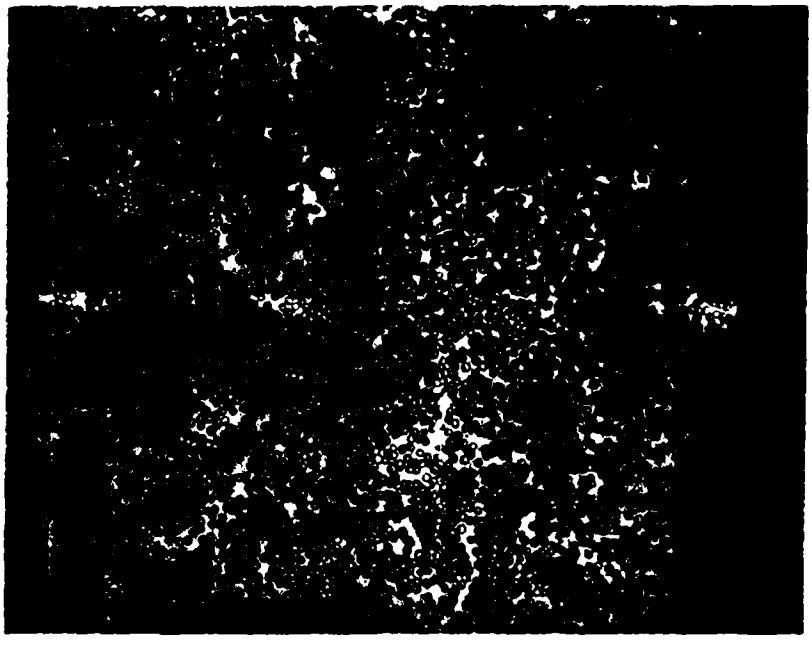

(c) 12 ply specimen, 100x.

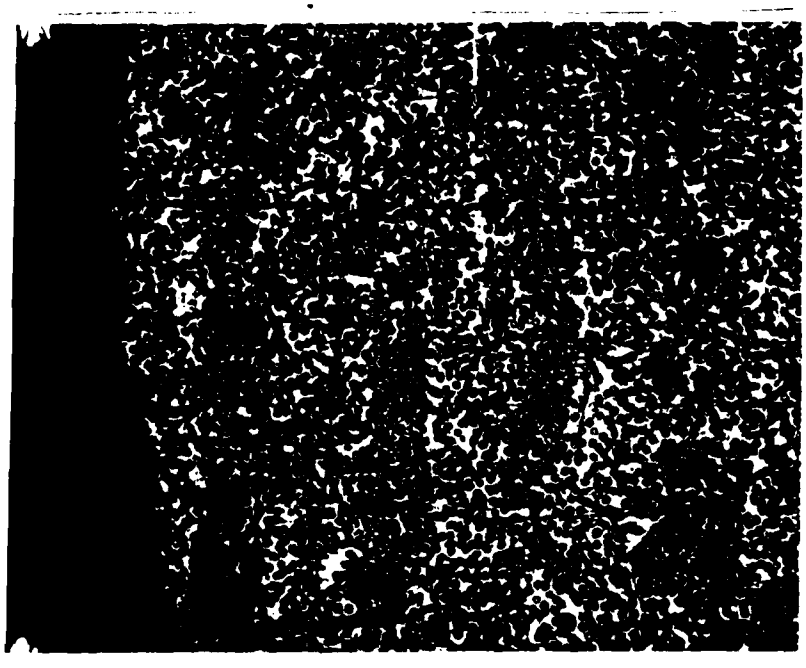

(d) 16 ply specimens, 100x.

Figures11a-11d (continued).